ADVANCED FUNCTIONAL MATERIALS
www.afm-journal.de

Visualized Atomic-Scale Manufacturing Using Transmission Electron Microscope

Mingrui Zhou, Chen Li, Hua Hong, Hubiao Huang, Qiubo Zhang, Kuibo Yin, Li Zhong, Chao Zhu, Tao Xu, and Litao Sun**

The relentless pursuit of device miniaturization and enhanced performance has driven manufacturing to its ultimate frontier—atomic-scale manufacturing. Despite recent advances, atomic-scale manufacturing as a whole remains in its infancy, largely constrained by the absence of direct visualization capabilities and a limited understanding of the underlying mechanisms. In situ transmission electron microscopy (TEM), with its exceptional spatiotemporal resolution and ability to integrate external fields, has emerged as a powerful platform that enables simultaneous fabrication and real-time observation. This review summarizes recent progress in visualized atomic-scale manufacturing using in situ TEM, with particular emphasis on processes mediated by electron beam irradiation, thermal excitation, and electrical bias under different environments. First, how an "atomic foundry" can be established inside the microscope through the application of external fields is examined. Subsequently, advances in visualized fabrication enabled by electron-beam engineering and external-field control are reviewed. Finally, key challenges and future perspectives are discussed, including the need for improved precision, higher throughput, and closer relevance to practical manufacturing conditions. Overall, this review underscores the pivotal role of in situ TEM in advancing the understanding and control of atomic-scale manufacturing, offering insights into precise atomic manipulation and pathways toward practical implementation.

1. Introduction

Manufacturing is the foundation of human civilization and socioeconomic development. The relentless pursuit of miniaturization and enhanced performance across diverse fields—including electronics,[1] communications,[2] biology,[3] and materials science[4] —is propelling manufacturing toward atomic-scale precision and functional feature sizes,[5] where manufacturing objectives and processes (removal, migration, or addition) directly focused on atoms, namely atomic-scale manufacturing. Devices and products fabricated through atomic-scale manufacturing techniques are expected to find broad applicability across a wide range of areas, including quantum computing,[6–8] advanced sensing,[9,10] high-density information storage,[11,12] energy conversion and storage, catalysis,[13–15] and numerous other emerging technological domains. For instance, positioning dopant atoms in Si crystals with atomic precision can enhance quantum bit stability, thereby promoting the implementation of quantum devices and advancing the development of quantum computers to meet the future demands for higher information processing capabilities and efficiency.[16,17] Likewise, manipulating individual atoms to encode bits can enable data-storage densities millions of times greater than those achievable with current solid-state memory technologies, which is essential for addressing the rapid growing demand for high-capacity information storage.[12,18] Atomic-scale manufacturing is also expected to enable the stable fabrication of atomic interferometric gyroscopes, which are theoretically predicted to be several orders of magnitude more sensitive than optical gyroscopes for inertial navigation applications.[19,20]

However, the advancement of such manufacturing faces enormous challenges, particularly using traditional manufacturing tools. As manufacturing scales down from the micro- and nanoscale to the atomic scale, it becomes a discrete process defined by the dimensions and positions of individual atoms, where even subtle structural variations can dramatically influence the properties and behaviors of materials.[21] At this scale, the phenomena of removal, migration, and addition can no longer be adequately explained by classical theories based on macroscopic statistical analysis, which treat processing objects as continuous media. Instead, the theoretical framework of atomic-scale manufacturing is rooted in quantum mechanics, making it fundamentally distinct from that of conventional manufacturing.

Although considerable efforts and investments have been devoted to advancing atomic-scale manufacturing, current approaches are either inefficient or lack sufficient accuracy. For instance, scanning probe microscope (SPM) can manipulate individual atoms or small clusters,[22] but it remains impractical

M. Zhou, C. Li, H. Hong, H. Huang, Q. Zhang, K. Yin, L. Zhong, C. Zhu, T. Xu, L. Sun
SEU-FEI Nano-Pico Center, Key Laboratory of MEMS of Ministry of Education
Southeast University
Nanjing 210096, China
E-mail: xt@seu.edu.cn; slt@seu.edu.cn

The ORCID identification number(s) for the author(s) of this article can be found under https://doi.org/10.1002/adfm.202526864

DOI: 10.1002/adfm.202526864

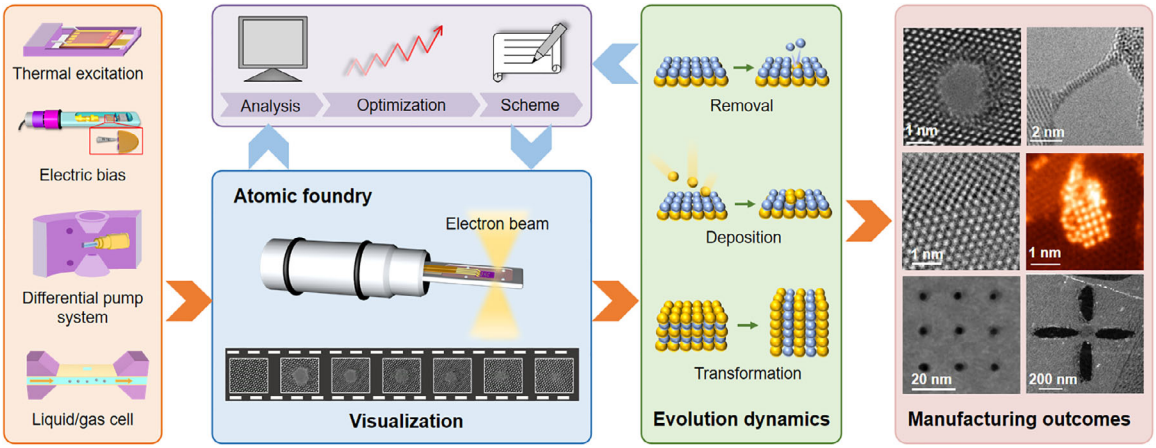

Figure 1. Schematic of visualized atomic-scale manufacturing using TEM. An atomic foundry is established within the microscope by applying external fields to replicate fabrication processes under various conditions, while analysis-based feedback is employed to guide the fabrication. These capabilities deepen the understanding of atomic-scale manufacturing mechanisms and provide new insights into potential pathways toward practical implementation. Reproduced with permission.[27] Copyright 2013, The Author(s). Reproduced with permission.[28] Copyright 2016, IOP Publishing Ltd. Reproduced with permission.[29] Copyright 2024, Elsevier Ltd. Reproduced with permission.[30] Copyright 2018, WILEY. Reproduced with permission.[31] Copyright 2022, The Authors.

for large-scale or high-throughput manufacturing.[23] Atomic layer deposition, chemical vapor deposition, and atomic layer etching provide atomic-layer precision in material addition and removal;[24] however, they still face substantial challenges in selectively depositing or removing atoms at specific, predetermined locations. Focused ion beam (FIB) machining and electron beam lithography are limited in achieving true single-atom precision or fabricating single-atom-scale feature sizes in substrates.[25,26] Overall, atomic-scale manufacturing remains in its early stages, and its further development relies on a comprehensive understanding of the underlying mechanisms.

At its core, atomic-scale manufacturing involves the subtraction, addition, or migration of atoms, atomic layers, or other atomic-scale structural units. Real-time observation of these processes is crucial for acquiring key information—such as structural transformations and the dynamic evolution of processed objects—that forms the fundamental for elucidating the mechanisms governing atomic-scale manufacturing. Moreover, such observations are essential for controlled manufacturing with atomic-scale precision.

Nowadays, both SPM and transmission electron microscope (TEM) enable atomic-scale characterization. However, SPM is less suitable for process monitoring because of the incompatibility between imaging and manipulation, coupled with its relatively low imaging speed. In contrast, TEM has garnered increasing attention owing to its superior spatial and temporal resolution, particularly when combined with advanced in situ techniques. Through instrument modifications or the use of dedicated sample holders, external stimuli and specialized environments—such as thermal excitation, mechanical force, electrical bias, and liquid or gaseous media—can be applied to materials with high precision, thereby extending TEM's capabilities to atomic manipulation. In addition, the electron beam, originally employed for imaging, can also be harnessed as a tool for processing. Consequently, an "atomic foundry" can be realized within the microscope (**Figure 1**), enabling the replication of fabrication under various conditions and the direct visualization of atomic-scale manufacturing. These capabilities facilitate a deeper understanding of atomic-scale manufacturing mechanisms and offer new insights into precise atomic manipulation and potential pathways toward practical implementation. This review highlights recent progress in visualized atomic-scale manufacturing using in situ TEM, with particular emphasis on processes mediated by electron beam irradiation, thermal excitation, and electrical bias under various environments. First, we delve into the establishment of an atomic foundry within the microscope, which is central to realizing and monitoring fabrication at the atomic scale. Next, we examine how an "atomic foundry" can be established inside TEM instrument through the application of external fields. Subsequently, recent advances in visualized fabrication achieved through in situ TEM are summarized, along with specific strategies and methodologies for atomic-scale processing. Finally, current challenges are outlined, and future perspectives in visualized atomic-scale manufacturing are discussed.

2. Atomic Foundry Inside a Transmission Electron Microscope

The integration of TEM with advanced in situ techniques has facilitated the establishment of a revolutionary "atomic foundry". This platform combines atomic-scale manipulation with real-time observation, thereby allowing direct visualization of atomic-scale manufacturing. In this section, we outline the fundamental principles and methodologies for constructing such an atomic foundry, with the aim of elucidating how atomic-scale manufacturing can be realized under diverse conditions within the TEM.

2.1. Electron-Matter Interactions and Electron Beam Irradiation

High-energy electron beams (typically 60–300 keV) constitute the foundation of TEM, with imaging fundamentally reliant on their

Table 1. Electron scattering and applications in manufacturing.

Scattering types	Effects	Processes	Outcomes	Refs.
Elastic scatterings	Displacement Sputtering	Sculpting	Nanopores	[36]
			Nanowires/Nanotubes	[27]
			Nanopatterns	[37,38]
		Manipulation	Nanodots	[39]
			Nanopatterns	[40]
Inelastic scattering	Charging Heating Radiolysis	Deposition	Nanoparticles	[41,42]
			Nanowires	[43]
			Nanosheets	[44]
		Oxidation growth	Nanoparticles	[45,46]
			Epitaxial layer	[47]
		Structural modification	Heterostructures	[48]

complex interactions with matter. As the electron beam penetrates the specimen, it interacts with the constituent atoms, giving rise to electron scattering. This scattering is generally categorized as either elastic or inelastic (**Table 1**), depending on whether energy is conserved. Elastic scattering, primarily governed by electrostatic interactions between incident electrons and atomic nuclei, can induce atomic displacements within the bulk or sputtering of surface atoms. In contrast, inelastic scattering—arising from Coulombic interactions between incident electrons and extranuclear electrons—can lead to effects such as electrostatic charging, localized heating, radiolysis and material deposition.[32] By leveraging these interactions, atomic-scale manufacturing can be realized with an electron beam, whether a parallel beam or a focused beam. Focused electron beam is particularly suitable for pattern sculpting, especially when it can be precisely directed at individual atoms with high density using a microscope operated in scanning TEM (STEM) mode or a dedicated STEM instrument, enabling atomic-scale manipulations.[33] In contrast, a parallel electron beam (operating in TEM mode) is better suited for large-area deposition, growth, and modification.[34,35] However, its selectivity is limited, as structural evolution under uniform electron beam irradiation is random.

Owing to its accessibility, atomic-scale manufacturing under electron beam irradiation can be carried out in any conventional TEM instrument. Electron-matter interactions are primarily governed by beam energy, electron dose, and dose rate. Consequently, by precisely adjusting parameters such as acceleration voltage, beam current, beam size, irradiation time, and exposure area, these interactions can be controlled, providing versatile strategies for electron-beam-based atomic-scale manufacturing. For example, elastic scattering can be effectively utilized for processing by setting the beam energy (acceleration voltage) above the threshold for atomic displacement. In graphene, electron beams above 80 keV enable stable and reproducible knock-on-based processing, allowing the fabrication of well-defined structures with atomic precision, as demonstrated in the formation of nanopores, nanoribbons, and other patterns on graphene membranes.[31,49] The tunability of acceleration voltage further enhances processing versatility. For instance, alternating between 100 and 60 kV has been employed to fabricate armchair nanoribbons and introduce silicon dopants on graphene.[50] Beyond elastic effects, inelastic scattering also plays a critical role in structural modification of semiconductor materials, particularly at beam energies below the atomic displacement threshold. For example, ionization effects can induce the formation of defects in MoS_2 under an 80 keV electron beam.[51,47] Notably, such an effect may be more pronounced as the acceleration voltage is further reduced within a specific range.[52]

2.2. Electrical Bias

The application of electric fields within TEM instruments opens new frontiers for probing and understanding electrically driven behaviors at the atomic scale. Currently, electric fields are primarily introduced via scanning tunneling microscopy (STM)-TEM systems or micro-electro-mechanical systems (MEMS)-based electric chips.[53] In STM-TEM systems, a high-precision piezoelectric actuator enables a probe to move along three axes with sub-angstrom accuracy relative to the sample mounted on the opposite side, providing access to structures ranging from the micrometer regime down to individual atomic chains. Upon contact between the movable probe and the sample, electrical characteristics such as current–voltage curves and current–distance profiles can be measured. In parallel, MEMS-based electric chips have also been widely employed to apply electric fields. In this case, the sample is transferred onto the chip, with its terminals connected to on-chip electrodes via FIB-assisted metal deposition. Compared with STM-TEM systems, MEMS-based chips offer superior measurement accuracy and stability. However, their high cost and time-intensive sample preparation remain significant limitations.

The ability to directly probe dynamic processes and elucidate their underlying mechanisms at the atomic scale provides a critical foundation for advancing atomic-scale fabrication under electric fields, which can be primarily regulated by varying field intensity and direction. For instance, electric-field-induced ion migration can be tracked with unprecedented spatiotemporal resolution, revealing ion-transport pathways and kinetics within complex material architectures. Similarly, electrically driven redox reactions—fundamental to electrocatalysis, corrosion, and

diverse synthetic pathways—can be directly visualized at atomic interfaces, providing critical insight into the precise atomic configurations that dictate chemical transformations. Electric fields also exert profound influence over phase transitions,[54–56] enabling real-time visualization of field-induced structural rearrangements and even the emergence of entirely novel phases. By elucidating the impact of electric fields on atomic migration, chemical bonding, and structural evolution, TEM studies provide critical knowledge for the atomic-level design of materials and devices. These insights open transformative opportunities for the rational engineering of functional materials, including the development of highly efficient catalysts through controlled active-site formation, advanced energy-storage components with optimized ion-transport pathways, and quantum devices via precise positioning of individual atoms or defects. The integration of real-time atomic-scale observation with programmable electric fields thus establishes a powerful pathway for advancing atomic-scale manufacturing under electrical stimuli.

2.3. Thermal Excitation

To visualize manufacturing under high-temperature conditions, it is essential to apply a tunable and stable temperature to the specimen inside a microscope without compromising imaging resolution. This is commonly achieved using a heating element integrated into the tip of the sample holder (referred to as a heating holder), which enables precise Joule heating and reliable temperature control. Heating holders are generally classified into two categories: furnace-type and MEMS-based. In furnace-type holders, conventional TEM grids are placed into a miniature electric furnace, offering simple sample preparation but often resulting in significant drift at elevated temperatures. Consequently, tens of minutes are typically required for stabilization, limiting the feasibility of atomic-resolution imaging of temperature-responsive processes. By contrast, MEMS-based heating holders have been widely adopted. In this configuration, a microfabricated heating chip is mounted into a compatible sample holder, with localized resistive heating generated by the passage of electric current through the chip. This approach provides several notable advantages, including high-precision temperature control (up to 0.01 °C), ultrafast heating and cooling rates (up to 10^5–10^6 °C s^{-1}), minimal drift, and excellent thermal stability, thereby enabling atomic-resolution imaging under dynamic thermal conditions.

This advanced methodology enables the dynamic investigation of various temperature-dependent phenomena at the atomic scale, primarily controlled through adjustments to target temperature, heating/cooling rate, and duration. For instance, material growth under thermal excitation can be directly examined,[57,58] allowing the nucleation and evolution of atomic clusters or layers to be precisely monitored and, in some cases, deliberately manipulated. It also facilitates the direct visualization of sublimation processes,[59–63] providing critical insights into the atomic-scale mechanisms governing material removal and structural reorganization under elevated thermal conditions. Furthermore, it is indispensable for probing phase transitions,[64–67] permitting real-time observation of structural rearrangements during thermally driven transformations. By enabling precise observation and control of temperature-dependent atomic dynamics—from the deposition of individual atoms during growth to lattice rearrangements during phase transitions—in situ heating delivers fundamental insights for atomic-scale fabrication under thermal excitation.

2.4. Liquid Environments

The introduction of liquid samples into TEM instruments presents significant challenges due to their high-vacuum environment, primarily because liquid evaporation under vacuum can severely disrupt stability and operation. Two principal strategies have been developed to address this while maintaining vacuum integrity in the microscope.

The first involves modifying the microscope's pumping system or using liquids with inherently low vapor pressure, allowing droplets to condense in an open environmental chamber. A differential pump system, typically used in an environmental TEM (ETEM), can gradually vary the pressure along the column, allowing the specimen chamber to be maintained at a relatively high pressure.[68] However, most liquids with high vapor pressures will still evaporate under these conditions. Although some liquid-phase experiments have been carried out in such systems,[69] they are primarily used for gas-phase studies.[70,71] Low-vapor-pressure ionic liquids, which can withstand the high vacuum of the TEM, have become increasingly popular for electrochemical characterization of nanobatteries, providing insights into charging and discharging processes.[72,73] Nevertheless, only a very small number of liquids can meet the stringent conditions for these experiments.

The second, more widely employed approach utilizes sealed liquid cells with electron-transparent windows to isolate the liquid from the vacuum, which is also applied to gas-phase experiments. However, this approach often degrades imaging resolution, as the window membrane introduces additional electron scattering. Consequently, the development of high-performance window has become a key focus in this field. Currently, various materials—including silicon nitride (SiN_x), amorphous carbon films, and 2D layered crystals[74–78]—have been utilized as liquid cell windows.

SiN_x windows have attracted considerable attention due to their mechanical robustness and compatibility with silicon-based microfabrication processes. The development of ultra-thin (<20 nm) SiN_x membranes enables sub-nanometer spatial resolution and facilitates real-time tracking of atomic-scale dynamics in liquid environments.[79] SiN_x-based liquid cells have proven to be a versatile platform for the in situ synthesis of diverse nanocrystals[80–82] and for monitoring kinetic pathways critical to nanofabrication in real time.[83,84] Amorphous carbon films have likewise been widely adopted for liquid encapsulation due to their straightforward fabrication and low cost. Typically, liquid samples are sandwiched between two TEM grids coated with carbon films, and subsequent solvent evaporation generates an encapsulated microenvironment, supporting investigations of processes such as oriented attachment,[85] etching,[86] and crystallization.[87] Meanwhile, graphene has emerged as a prominent window material for liquid cells due to its intrinsic atomic thickness, which minimizes electron scattering and enhances

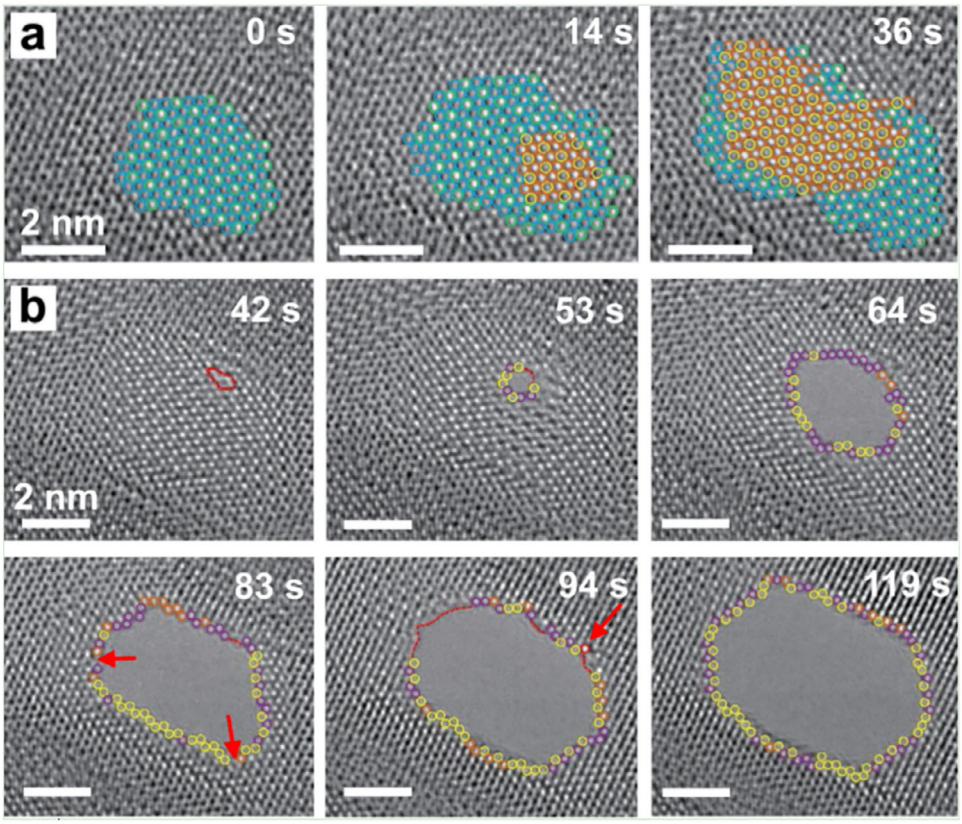

Figure 2. Nanopore fabrication in a Bi_2Te_3 substrate using 300 keV electron beam.[99] a) Electron beam-induced thinning of Bi_2Te_3 to a monolayer. b) Nucleation and structural evolution of a nanopore within the Bi_2Te_3 monolayer. Dotted lines and circles indicate different edge configurations, and arrows mark defects. Reproduced with permission.[99] Copyright 2022, Tsinghua University Press and Springer–Verlag GmbH Germany, part of Springer Nature.

spatial resolution, and its exceptional mechanical strength, which prevents window rupture. Graphene-based liquid cells have facilitated real-time observation of structural evolution with atomic resolution.[88,89] Beyond graphene, other 2D layered materials, such as MoS_2, have also been employed as liquid cell membranes, demonstrating excellent performance for probing fabrication in liquid environments.[90,91]

3. Atomic-Scale Manufacturing under Various Conditions

3.1. Atomic-Scale Manufacturing under Electron Beam Irradiation

The electron microscope offers a powerful platform for atomic-scale manipulation via electron-matter interactions, enabling the removal, migration, and addition of atoms. These phenomena manifest as etching, reconstruction, and growth at the atomic scale under electron beam irradiation.

3.1.1. Electron Beam-Induced Etching

Numerous studies have demonstrated that electron beam-induced etching offers a top-down approach for fabricating novel structures, typically arising from mechanisms such as knock-on displacement, sputtering, ionization, and electron beam-induced chemical etching.[92] At the atomic scale, it generally involves defect formation and atom removal. Our previous work demonstrated the formation of defect structures under electron beam irradiation,[93–95] and achieved direct visualization of atom-by-atom etching at nanocrystal edges.[96] Other groups have also investigated electron beam-induced defect formation and its underlying mechanisms in detail, also indicating the electron beam as a versatile tool for atomic manipulations.[38,97] In general, single-atom vacancies can be generated by carefully controlling beam intensity, beam size, and irradiation time.[98] Since unsaturated atoms at defect edges are more susceptible to displacement than fully coordinated atoms without dangling bonds, continued irradiation can be deliberately applied to progressively enlarge vacancies, enabling controlled nanopore fabrication. **Figure 2** illustrates the fabrication of nanopores in a Bi_2Te_3 substrate with precise edge-configuration control.[99] The process was initiated by deliberate thinning of the target region under 300 keV electron beam, which drove the structural evolution from multilayer to monolayer (Figure 2a). Continuous irradiation subsequently induced nanopore nucleation within the monolayer (Figure 2b). Prolonged exposure progressively enlarged the nanopore, accompanied by increasing edge structural complexity and the emergence of diverse atomic configurations, primarily zigzag and flat

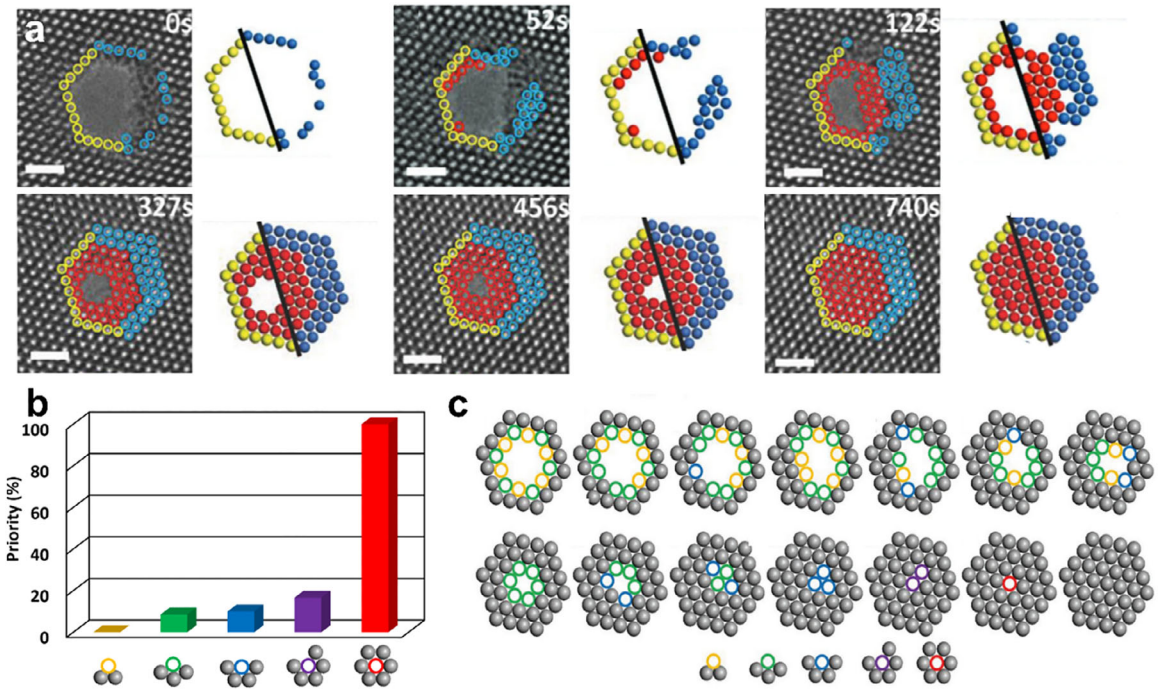

Figure 3. Electron beam-induced structural repair in MoS_2.[30] a) TEM image sequence showing nanopore healing in MoS_2 under electron beam irradiation with a beam current density of 10^5 A m^{-2}. Yellow and blue circles label crystalline and amorphous edges, respectively, while red circles indicate newly repaired channels. Scale bar: 1 nm. b) Priority diagram illustrating site occupancy preference. The orange, green, blue, purple, and red circles correspond to sites enclosed by two, three, four, five, and six channels, respectively. c) Schematic illustration of the repair mechanism. Reproduced with permission.[30] Copyright 2018, WILEY.

edge types. Extended irradiation further increased the proportion of zigzag edges. Given that distinct edge structures exhibit markedly different electronic properties, these findings indicate that electron beams can not only modulate structural configurations but also tailor the associated properties.

More recently, the integration of deep learning to guide electron beam trajectories has enabled the fabrication of patterns with predefined geometries and edge configurations.[37,100–102] This advancement significantly enhances the capabilities of electron probes as direct-write tools, facilitating the fabrication of structures with architectural complexity and unique functionalities.

Although fabricating devices inside an electron microscope remains challenging due to limited operational flexibility, the creation of structures with atomic precision as building blocks for devices is highly attractive. As the most promising building blocks for future electronic devices, ultrathin 1D structures can be fabricated between adjacent nanopores. The initial width of a 1D structure depends on the distance between nanopores, and further thinning under electron beam irradiation enables the fabrication of sub-nanometer wires and even atomic chains within the substrate.[103] Following this strategy, it is found that wires ≈0.4 nm wide can be derived from MoS_2 monolayers, which remain robust under electron beam irradiation and are clearly distinct from the parent structures.[27] Similar 1D structures can also be created in other transition metal dichalcogenides (TMDCs) sheets, exhibiting metallic properties suitable for use as nanoscale interconnects.[104] Likewise, nanoribbons can form between two adjacent pores in bilayer sheets and can transform into single-walled tubular structures when the dangling bonds at the edges are saturated through interlayer bonding. Xu et al. demonstrated that nanotubes can be fabricated in AA'-stacked bilayer *h*-BN, with their diameters precisely modulated by sequentially removing atomic rows under sustained irradiation.[105]

3.1.2. Electron Beam-Induced Reconstruction

It is noteworthy that most displaced surface atoms remain as adatoms rather than leaving the specimen immediately. The surface diffusion of these atoms, followed by reconstruction at energetically favorable sites, is facilitated under electron beam irradiation due to their relatively low activation energy. Such reconstructions can generally be classified into two categories: i) atomic rearrangement toward the parent structure, such as structural repair through localized ordering, and ii) phase transformations involving alterations in crystal structure or chemical composition.

Electron beam-induced structural repair has been demonstrated in a variety of material systems.[30,106,107] Notably, electron beam irradiation can simultaneously induce both damage and repair, with the relative rates of these processes governed by the beam intensity. Therefore, precise control of beam intensity is critical to achieving an optimal balance between sculpting and healing. **Figure 3** illustrates an example of such repair in a MoS_2 membrane.[30] A nanopore was first drilled using a 300 keV focused electron beam, followed by lattice reconstruction under moderate parallel-beam irradiation with a beam current density of 10^5 A m^{-2}. As shown in Figure 3a, the initially

amorphous region on the right side of the nanopore gradually reconstructs into an ordered lattice, primarily driven by the diffusion and rearrangement of S atoms together with Mo atoms aggregated within the amorphous region. In contrast, the left side of the nanopore exhibits slower healing. Statistical analyses indicate that atomic sites surrounded by a greater number of neighboring columns are more likely to be occupied and remain more stable after adatom attachment (Figure 3b). Accordingly, the repair behavior conforms to the Kossel–Stranski model, in which adatoms preferentially occupy sites with higher coordination (Figure 3c).

Electron beam-induced phase transformations involve changes in crystal structure or elemental composition and have been observed across a wide range of material systems. A stable crystalline structure can be disrupted by the electron beam, producing a metastable amorphous phase, whereas metastable amorphous materials can also be crystallized under controlled electron beam irradiation.[108,109] For instance, amorphous carbon supported on flat 2D sheets can be graphitized under 80 keV electron beam irradiation into a planar structure parallel to the support sheet.[110] Similarly, amorphous MoS_2 can be crystallized and restructured into crystalline domains using either 80 or 200 keV electron beams, effectively emulating conventional high-temperature synthesis and processing conditions.[111] Building on this foundation, atomic-level sculpting of three-dimensional (3D) crystalline structures from metastable amorphous films can be achieved using an atomically focused electron beam. By precisely controlling the beam position and scan speed, arbitrary-shaped structures with features as small as 1–2 nm can be fabricated, enabling a complementary bottom-up approach to 3D printing.[112]

Beyond crystallization from amorphous phases, transformations between distinct crystalline phases can also be achieved by electron irradiation.[113–117] A representative example is the beam-driven transformation from semiconducting 2H-MoS_2 to metallic 1T-MoS_2 via lattice-plane gliding.[110,118] The transformation begins with the formation of an α-phase precursor consisting of three or four constricted zigzag chains, followed by local strain-induced gliding of S planes or Mo—S atomic layers when two non-parallel α-phases are in contact. Consequently, a triangular nucleus of the 1T phase forms and expands through the migration of a β-boundary. Such a transformation only occurs in the irradiated region, enabling spatially selective phase engineering through precise control of the electron beam.

Irradiation-induced compositional changes are frequently observed in compounds containing multiple elements. Naturally, the elemental ratio may vary if the rate of atomic loss differs from the initial stoichiometry of the specimen, making phase transformations between compositions with distinct stoichiometries feasible under electron irradiation.[35,119] For instance, 2D in-plane heterostructures have been successfully fabricated through irradiation-induced phase transformation in TMDCs, in which the transformed phases were seamlessly integrated with the pristine region, yielding ultraclean and atomically sharp heterointerfaces.[29] **Figure 4** presents a representative example of the transformation from a hexagonal to a tetragonal lattice in a MoS_2 sheet. This transformation initiates with the formation of sulfur vacancies, which subsequently aggregate into line defects, inducing local lattice contraction and strain accumulation that drive reconstruction into a stable tetragonal phase identified as metallic MoS. These results demonstrate that electron beam irradiation enables precise, site-selective engineering of in-plane heterostructures.

3.1.3. Electron Beam-Induced Growth

It has been demonstrated that electron irradiation can trigger the nucleation and growth of nanostructures. Successful realization of such growth within a microscope depends on the careful selection of suitable precursors, which can be introduced into the vacuum specimen chamber and released in sufficient quantities to facilitate the formation of the desired structures. Gas residues within the column and surface adsorbates on specimens or TEM grids can serve as potential feedstocks, supplying small amounts of oxygen for oxidation growth. A representative example is the controlled growth of metal oxides under electron beam irradiation.[47,120,121] As shown in **Figure 5a**, pronounces oxidation occurs exclusively in the irradiated regions of the Ag nanowires, where new oxide crystals nucleate on the surface and subsequently grow through lateral extension and vertical thickening, characteristic of a layer-by-layer growth mode (Figure 5b). The outward surface diffusion of Ag atoms, coupled with the ionization of oxygen molecules under electron irradiation, plays a crucial role in the oxidation growth. It is worth noting that increasing the electron beam density can induce the reduction of Ag_2O back to metallic Ag, demonstrating the exceptional controllability of electron-beam-induced growth.[46] In addition, oxidation growth is also affected by beam energy, as demonstrated by the oxidation of In nanoparticles. Yolk-shell particles preferentially form under 200 keV electron beam irradiation, with oxidation kinetics consistent with the Cabrera–Mott theory, whereas hollow particles are predominantly formed under 300 keV irradiation.[120] These works confirm that electron beam irradiation is a powerful tool for the controlled engineering and modification of materials.

Another common strategy is to induce nanostructure growth using substrate templates, where the growth precursors originate directly from residual clusters on the specimen surface. Yin et al. employed a 60 keV focused electron beam to directly fabricate monolayer CuO architectures within graphene nanopores and on graphene substrates.[28] Parallel beams have also been widely used to fabricate free-standing, atomically thin crystals within nanopores or epitaxial atomic layers on 2D substrates.[122–125]

3.2. Atomic-Scale Manufacturing under Electric Bias

3.2.1. Fabrication of Heterostructures

Electric field-driven atomic migration has emerged as a powerful strategy for the fabrication of diverse nanostructures. Qu et al.[126] successfully fabricated stable 1D Ag atomic chains by applying an electric field to induce Ag atom migration between two Ag nanocrystals under simultaneous tensile loading. Systematic investigation of room-temperature piezoresistance in these atomic chains under varying atomic spacings and strain levels revealed a strong potential for nanoscale strain-sensing applications. Similarly, Yuk et al.[127] developed a rapid fabrication strategy for 0D

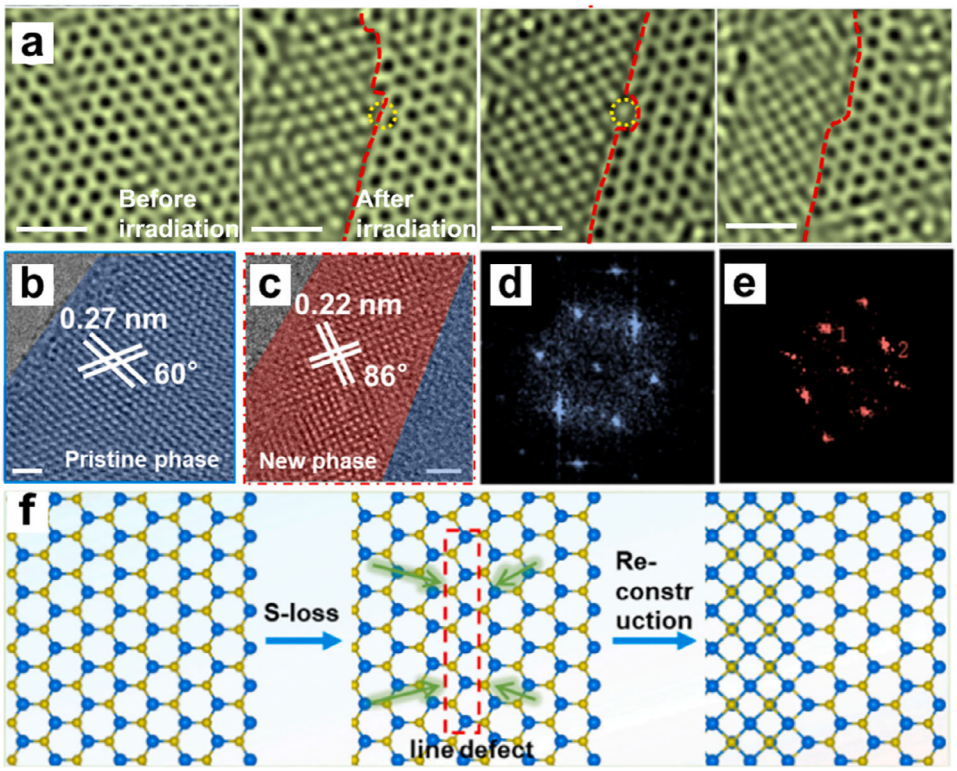

Figure 4. Electron beam-induced phase transition in MoS_2.[29] a) Structural evolution under 80 keV electron beam irradiation with a dose rate of 6.7×10^6 e nm^{-2}·s. The red dashed line indicates the transition frontier. Scale bar: 1 nm. b,c) High-resolution TEM (HRTEM) images before and after irradiation. Scale bar: 1 nm. d,e) Corresponding fast Fourier transform (FFT) patterns of (b) and (c). f) Schematic illustration of the phase transition mechanism. Reproduced with permission.[29] Copyright 2024, Elsevier Ltd.

and 1D Zn nanostructures. By applying an external voltage across ZnO thin films, they utilized Joule heating-assisted electromigration to extract Zn ions from the films, thereby enabling the controlled growth of Zn structures. This method allowed precise control over the size, morphology, and spatial distribution of the resulting nanostructures on the ZnO films.

Furthermore, atomic diffusion has also been recognized as a powerful approach for the preparation of heterostructures. Zhang et al.[128] reported an electrically driven, diffusion-controlled solid-solid reaction inside a STM-TEM system, achieving controllable fabrication of two distinct Ag–Te heterostructures—core-shell and segmented configurations—through voltage modulation (**Figure 6**a). The formation dynamics of the Ag–Ag_2Te core-shell structure was resolved with atomic-scale precision, revealing a two-stage growth process: initial nucleation and growth of nanoscale hillocks, followed by their coalescence and thickening (Figure 6b). Conversely, reversing the voltage polarity led to the formation of a segmented Ag_2Te–Te heterostructure (Figure 6c,d). The formation of these two types of heterostructures relies on distinct atomic migration pathways, where electrostatic forces (F_i) and electron-wind forces (F_s) jointly determine the direction of atom migration (Figure 6e). Under positive voltage bias, surface diffusion of Te atoms from Te nanowires toward Ag nanowires drives the formation of a core-shell structure. In contrast, under negative voltage bias, Joule heating-induced temperature rise can activate bulk diffusion of Ag atoms from Ag nanowires, resulting in the formation of a segmented heterostructure.

Cation exchange (CE) reactions have also been established as a powerful synthetic strategy for creating heterogeneous nanomaterials through controlled cation substitution,[129,130] directly contributing to advances in atomic-scale manufacturing. Zhang et al.[131] reported an electrically driven CE approach for fabricating sulfide nanostructures within an STM–TEM system, uniquely enabling atomic-resolution monitoring of dynamic reaction processes crucial for atomic-precision manufacturing (**Figure 7**). The experimental configuration consisted of a Cu/CdS nanowire/W structure (Figure 7a) and was thoroughly characterized using selected area electron diffraction (SAED), current-voltage (I–V) measurements, and elemental mapping (Figure 7b–e). Notably, the application of a voltage bias induced the formation of a CdS–Cu_2S core-shell structure, as verified through comprehensive structural and compositional analyses (Figure 7f–o). Elemental mappings of Cd and Cu, captured at different stages, revealed critical details of the core-shell structure evolution (Figure 7p). This electrically mediated CE method offers precise control over nanocrystal synthesis through bias modulation, demonstrating significant potential for engineering complex nanostructures with atomic precision. By combining real-time monitoring with selective CE, this approach represents a major advancement toward atomic-scale manufacturing and the rational design of tailored nanomaterials.

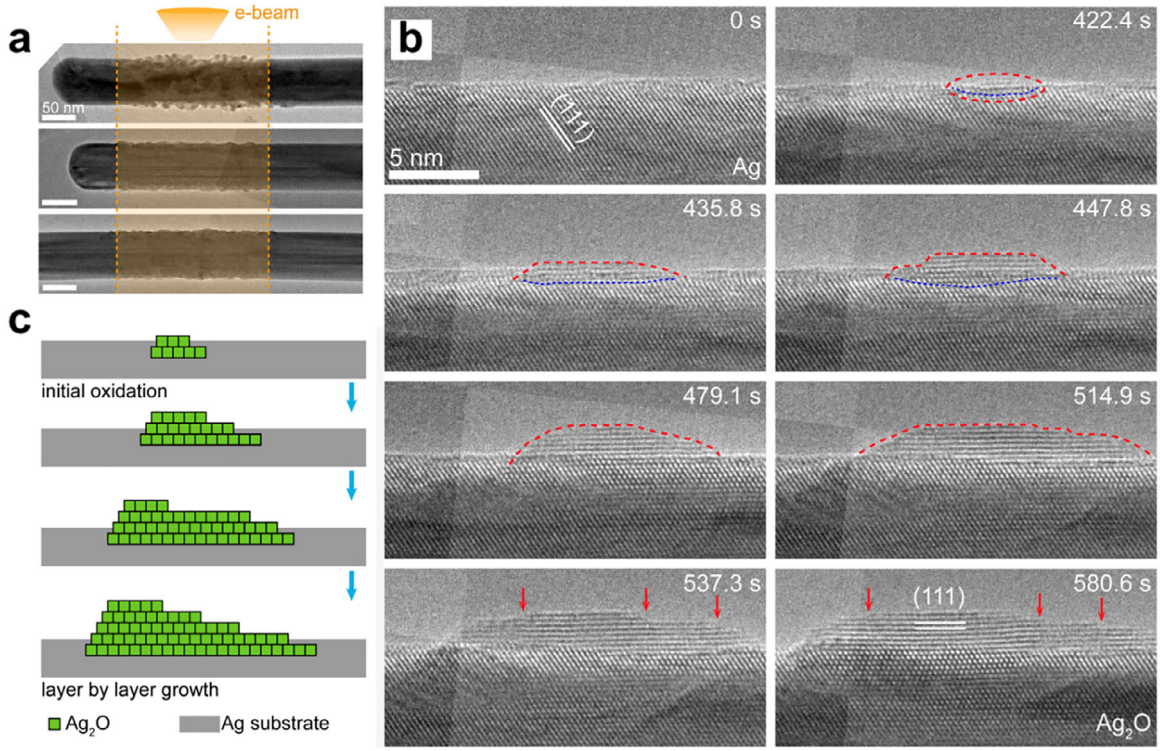

Figure 5. Electron beam-induced oxidation growth.[47] a) Morphological evolution only occurs in the regions exposed to electron beam. b) The growth dynamics of Ag_2O grain at a dose rate of 10 700 e $Å^{-2}$ s^{-1}. Arrows indicate step edges of individual oxide layers, while dashed lines mark the interface. c) Schematic illustration of the layer-by-layer growth mechanism. Reproduced with permission.[47] Copyright 2021, The Author(s), published by MDPI.

In addition, controlled atom (or ion) diffusion mechanisms provide a fundamental basis for the atomic-level construction of heterostructures and the precise engineering of hetero-phase nanostructures. In multiphase layered materials, a key strategy involves lowering the energy barriers for phase transformations through intercalation of alkali metal ions,[132–138] which enables controlled structural phase transitions and the formation of hetero-phase architectures at the atomic scale. Chen et al.[139] reported a 2H-1T' phase transition in MoS_2 induced by lithium intercalation, where superlattice structures emerged as lithium ions were inserted, demonstrating the potential to reconstruct the internal atomic arrangement of materials through ion intercalation. Fu et al.[140] employed an STM-TEM system to control the sodiation of 3R-NbS_2 nanoplatelets (**Figure 8**a,b). As Na^+ ions intercalated, a reaction front boundary propagated continuously (Figure 8c–f). HRTEM images (Figure 8g–j) and corresponding FFT patterns (Figure 8k,l) acquired before and after sodiation confirmed a phase transition from 3R–NbS_2 to 2H–$NaNbS_2$. By precisely controlling the sodiation time, atomic-level control over both phase composition and structure can be achieved, allowing the formation of 3R–2H hetero-phase nanoplatelets or fully transformed 2H–$NaNbS_2$ nanoplatelets.

3.3. Atomic-Scale Manufacturing under Thermal Excitation

The advent of in situ TEM has revolutionized the ability to probe morphological and structural transformations under precisely controlled thermal excitation. By combining real-time atomic resolution imaging with pulsed heating techniques, researchers can elucidate the fundamental mechanisms governing sublimation-induced morphological evolution. Shangguan et al.[141] reported size-dependent sublimation behaviors in Te nanowires. As shown in **Figure 9**a, the sublimation of a Te nanowire, viewed along the [10$\bar{1}$0] direction, exhibits a clear layer-by-layer disappearance of Te atoms from the sublimation surface. Notably, pulsed heating enables precisely controlled sublimation of electron-beam-patterned trapezoidal-notch Te nanowires, with sublimation preferentially occurring from the side surfaces rather than the nanowire termini, as shown in Figure 9b–d. Detailed analysis revealed that the morphological evolution during sublimation is governed by interfacial wetting equilibrium and crystallographic orientation, which ultimately determine whether spherical surfaces or well-defined faceted structures form at exposed surfaces. This insight is vital for predicting and controlling material removal under thermal excitation at the atomic scale.

Similarly, Li et al.[60] employed aberration-corrected TEM to directly observe atomic-scale sublimation kinetics in silver nanoparticles, providing crucial insights for precise atomic fabrication. Atomic-level observations reveal how particle size, surface characteristics, and defects govern this first-order phase transformation. Through atomic-resolution imaging during thermal treatment, they demonstrated that Ag nanoparticles smaller than ≈30 nm preferentially expose stable {100} facets during sublimation—a critical insight for controlling atomic

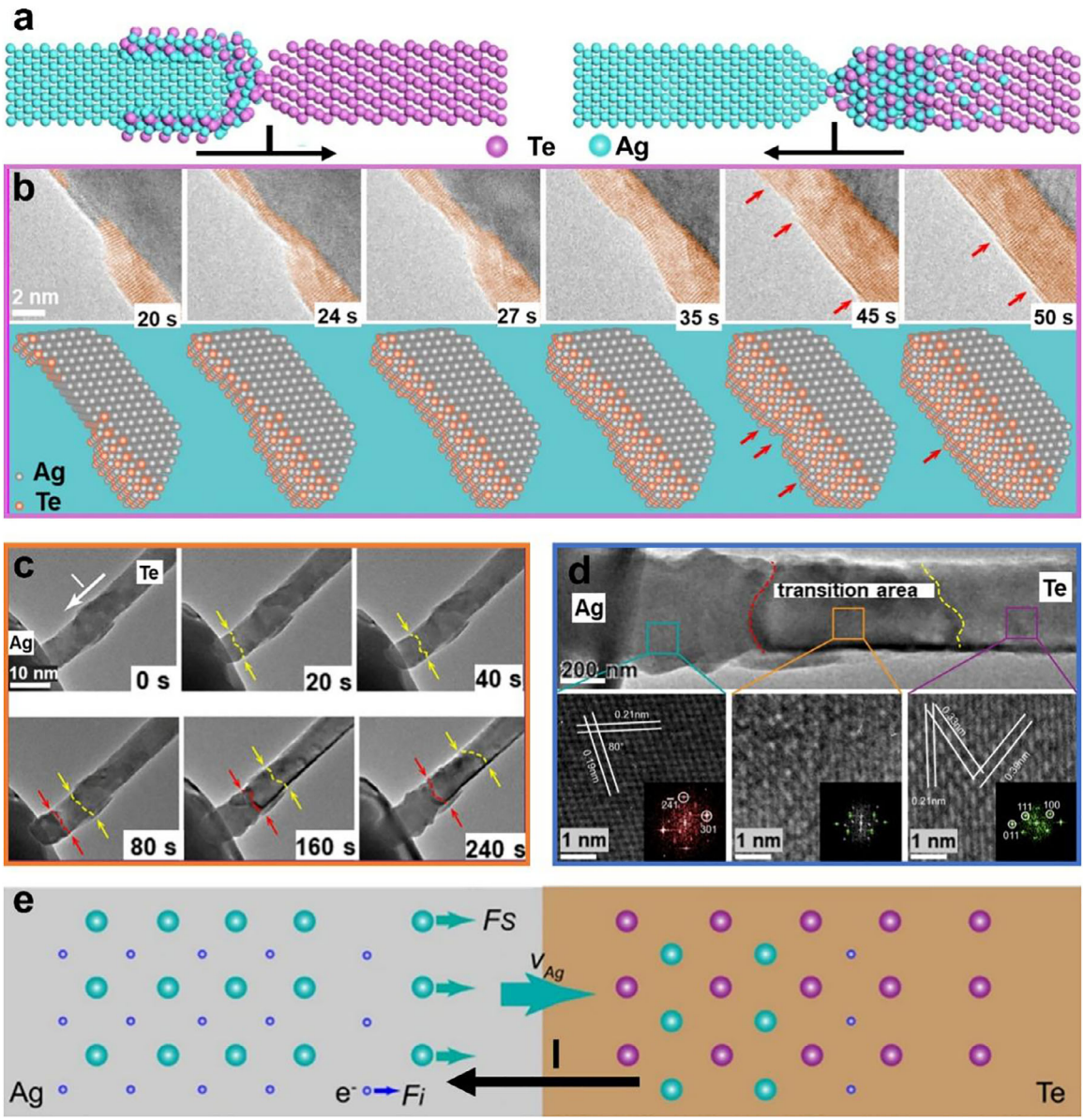

Figure 6. Fabrication of diverse heterostructures through electrically driven atomic migration.[128] a) Schematic illustration depicting the formation of Ag–Ag_2Te core-shell structured nanowire and segmented Ag_2Te-Te structured nanowire under opposite electric field polarities. b) Formation process of Ag–Ag_2Te core-shell structure under a positive voltage bias. Arrows indicate the progressive growth of the Ag_2Te layer. c) Evolution of segmented Ag_2Te–Te heterostructure under a negative voltage bias (−0.8 V). Yellow lines delineate the diffusion frontier, while the red lines indicate the phase transformation frontier. d) Fully formed segmented Ag_2Te–Te heterostructure. The bottom panels present HRTEM images and corresponding FFT patterns acquired from distinct regions along the heterostructure. e) Schematic illustration of the forces acting on the Ag–Te system under a negative bias. Reproduced with permission.[128] Copyright 2021, The Author(s), Published by Springer Nature.

arrangements in fabrication. Furthermore, two distinct sublimation pathways were identified: uniform sublimation predominates in particles with low surface energy, whereas high-energy systems or particles containing 5-fold twin boundaries exhibit nonuniform sublimation patterns. Dynamic analysis further established a critical size threshold of ≈8 nm, where sublimation rates transition from linear to nonlinear behavior in both pathways. These findings collectively demonstrate the precise control achievable in the manipulation of geometry and defect structure, paving the way for the fabrication of tailored materials and devices at the ultimate atomic limit.

Beyond morphology control via thermal sublimation, recent advances have extended thermal modulation to phase engineering in 2D materials, demonstrating potential for the atomic-scale manufacturing of heterostructures. Wang et al.[142] used TEM with a heating holder to achieve the 2H-to-1T'phase transition in $MoTe_2$ at 880 °C, creating a lateral homojunction of 1T'-enriched and 2H $MoTe_2$ by controlling Te sublimation through h–BN

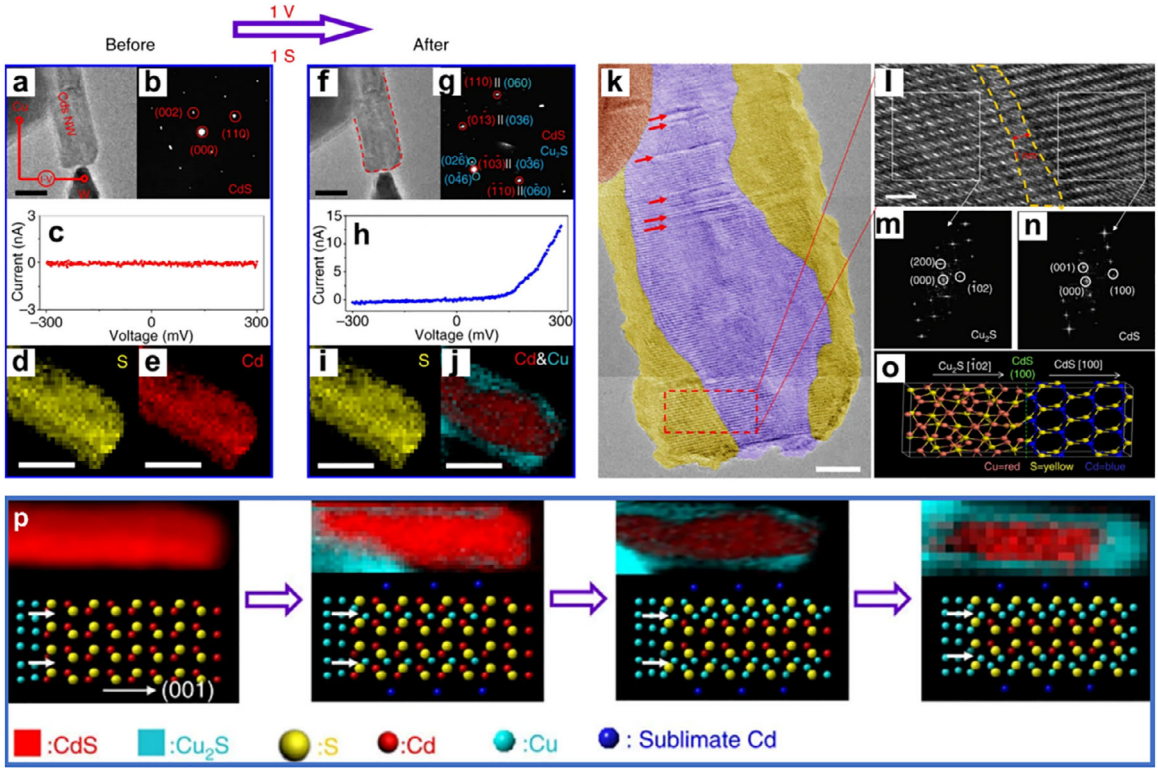

Figure 7. Fabrication of core-shell nanowires via electrically driven cation exchange.[131] a–e) Characterization of the nanowire before biasing: (a) low-magnification image of the experimental setup, (b) SAED pattern, (c) *I–V* curve, and (d, e) corresponding elemental mapping images. f–j) Characterization of the nanowire after biasing under 1 V voltage for 1s: (f) TEM image, (g) SAED pattern, (h) *I–V* curve, (i, j) elemental mapping images. Scale bar: 50 nm. k) TEM image of the CdS-Cu_2S heterostructure nanowire. Scale bar: 10 nm. l) Enlarged image of the region in (k). Scale bar: 2 nm. (m, n) The FFT patterns from the left and right sides of the interface in (l). o) Schematic illustration of the CdS-Cu_2S heterostructure. p) Elemental mapping images and corresponding structures at different stages of core-shell formation. Reproduced with permission.[131] Copyright 2017, The Author(s), Published by Springer Nature.

coverage on targeted regions. Similarly, Lee et al.[143] achieved reversible phase transition between 2H and the T_d phases in few-layer $MoTe_2$ using laser irradiation and thermal annealing, showcasing a pathway for atomically precise phase control. Through in situ pulsed heating, they observed the T_d-to-2H phase transition initiating at temperatures as low as 200–225 °C. Liao et al.[144] demonstrated the 2D-to-1D transformation of 2H–$MoTe_2$ nanosheets into Mo_6Te_6 nanowires under Mo-rich conditions, proceeding through metastable $Mo_{1+x}Te_2$ and Mo_6Te_6. Sequentially, 2H–$MoTe_2$ converts to M–$Mo_{1+x}Te_2$ through Mo intercalation, then to M–Mo_6Te_6 via Mo substitution, followed by lattice relaxation to form Mo_6Te_6 nanowires.

Thermally driven decomposition can also serve as an atomic-scale manufacturing strategy. This approach is founded on three key insights: 1) thermally activated atomic migration follows predictable pathways guided by crystalline templates; 2) decomposition byproducts act as feedstock for targeted structure growth; and 3) real-time TEM visualization enables feedback-controlled fabrication with atomic-scale precision. Yu et al.[145] achieved epitaxial graphene growth on a SiC surface at 1000 °C. Atomic-resolution observations revealed that sequential decomposition of three SiC (1$\bar{1}$00) layers generates carbon clusters and chains that progressively nucleate, connect, and fill pores, ultimately forming a continuous graphene monolayer (**Figure 10a–l**). Detailed analysis of the evolving interlayer distance between the emerging carbon layer and the SiC surface further confirmed the stepwise structural transformations (Figure 10m).

Another example is the decomposition of body-centered tetragonal PX-$PbTiO_3$ nanowires,[34] achieved via in situ electron beam irradiation combined with thermal treatment in TEM. Extended heating progressively degraded the crystalline structure, leading to amorphization (**Figure 11a**). Temperature modulation enabled tunable structural evolution: at 300 °C, the transformation produced amorphous nanowires decorated with liquid Pb nanoparticles (Figure 11b–e), while at 500 °C, the amorphous phase crystallized into porous TiO_2 structures (Figure 11f,g). Essentially, spatially localized electron-beam positioning enables crystallization within predefined regions of the nanowires. This work not only elucidates the phase transformation kinetics from PX-$PbTiO_3$ to monoclinic TiO_2 but also establishes a framework for crystallographic engineering.

Thermal decomposition has also served as a powerful approach for fabricating high-performance electrocatalysts. Wang et al.[146] achieved thermal assembly of Pt nanostructures through precursor decomposition on monolayer MoS_2, enabling precise spatial registration. Their strategy deterministically positioned single Pt atoms with sub-angström precision, guided controlled aggregation into nanocrystals exhibiting two distinct epitaxial

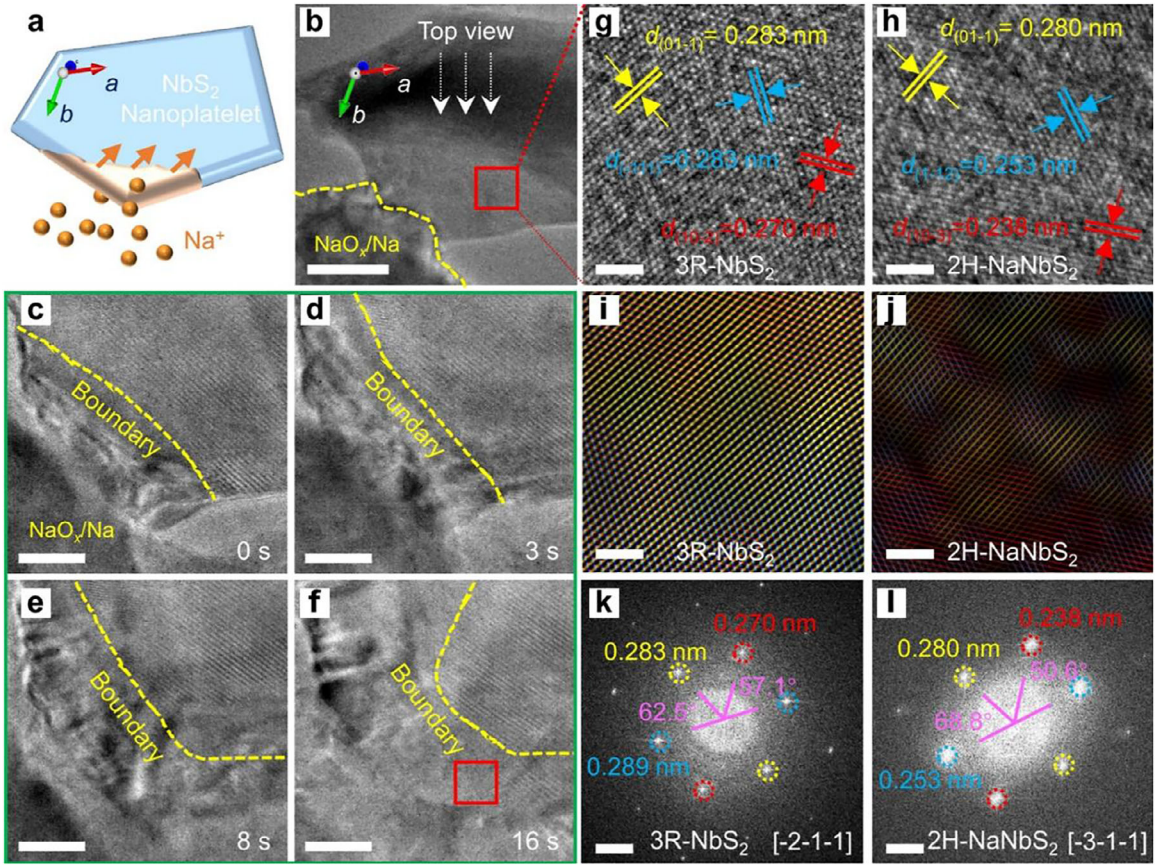

Figure 8. Fabrication of heterostructures through electrically driven Na^+ ions intercalation.[140] a) Schematic illustration of Na^+ ion intercalation into layered materials. b) TEM image of the contact interface between NbS_2 and Na. Scale bar: 200 nm. c–f) Morphological evolution of a NbS_2 nanoplatelet during electrochemical sodiation. Scale bar: 50 nm. g) TEM image of the pristine NbS_2 nanoplatelet, acquired from the rectangular region in (b). h) TEM image of the sodiated NbS_2 nanoplatelet, obtained from the marked region in (f). i,j) Corresponding filtered images of (g) and (h), respectively. Scale bars: 2 nm. k,l) FFT patterns of (i) and (j), respectively. Scale bars: 1 nm^{-1}. Reproduced with permission.[140] Copyright 2024, American Chemical Society.

relationships with the MoS_2 lattice (registry error < 2°), and produced strain-engineered Pt monolayers with a 7–10% lattice expansion relative to bulk Pt. This work unveiled three phenomena relevant to atomic-scale manufacturing: carbon-mediated confinement stabilizes single Pt atoms at elevated temperatures; non-equilibrium electron beam effects enable atomic-scale patterning of the MoS_2 substrate; an amorphous carbon matrix preserves the Pt–MoS_2 interfacial registry while suppressing local etching.

3.4. Atomic-Scale Manufacturing in Liquid Environment

The development of liquid cell TEM (LCTEM) enables real-time visualization and regulation of material processing within liquid environments. In a liquid cell, both etching and growth are governed by the combined effects of solution chemistry and electron beam irradiation. Under beam exposure, radiolysis of aqueous solutions generates reactive species, such as e_h^-, H•, OH•, H_2, H_2O_2, O_2, and HO_2•.[147] Among those, oxidizing species (e.g., OH• and H_2O_2) drive atomically precise etching of metals in aqueous solution by promoting their oxidation to metal ions,[148] whereas reducing species (e.g., e_h^- and H•) facilitate the reduction of metal ions, enabling local growth or selective plating. Therefore, precise control of the chemical environment in solution is crucial for regulating kinetic processes. In general, increasing the temperature can elevate the relative concentration of redox agents in the solution.[149] The introduction of radical scavengers and adjustments of beam dose are expected to mitigate the radiolysis.[150] The solution composition also plays a decisive role in determining etching behaviors. For instance, by adjusting the concentration of $FeCl_3$ and $Fe(acac)_3$, Zheng et al. modulated the etching behavior of Pd nanocrystals.[151] At low $Fe(acac)_3$ concentrations, preferential etching of Pd(100) facets produced concave morphologies, whereas higher concentrations reduced the etching rate due to the formation of a protective $Fe(acac)_3$ film on {100} facets, resulting in spherical morphologies. These findings demonstrate that liquid-phase fabrication can be precisely controlled through careful adjustment of parameters such as electron beam dose rate, solution composition, and solution concentration.

Realizing the nucleation, growth, and assembly of nanocrystals represents a key application of LCTEM, enabling the rational design of nanomaterials with tailored structures and properties.

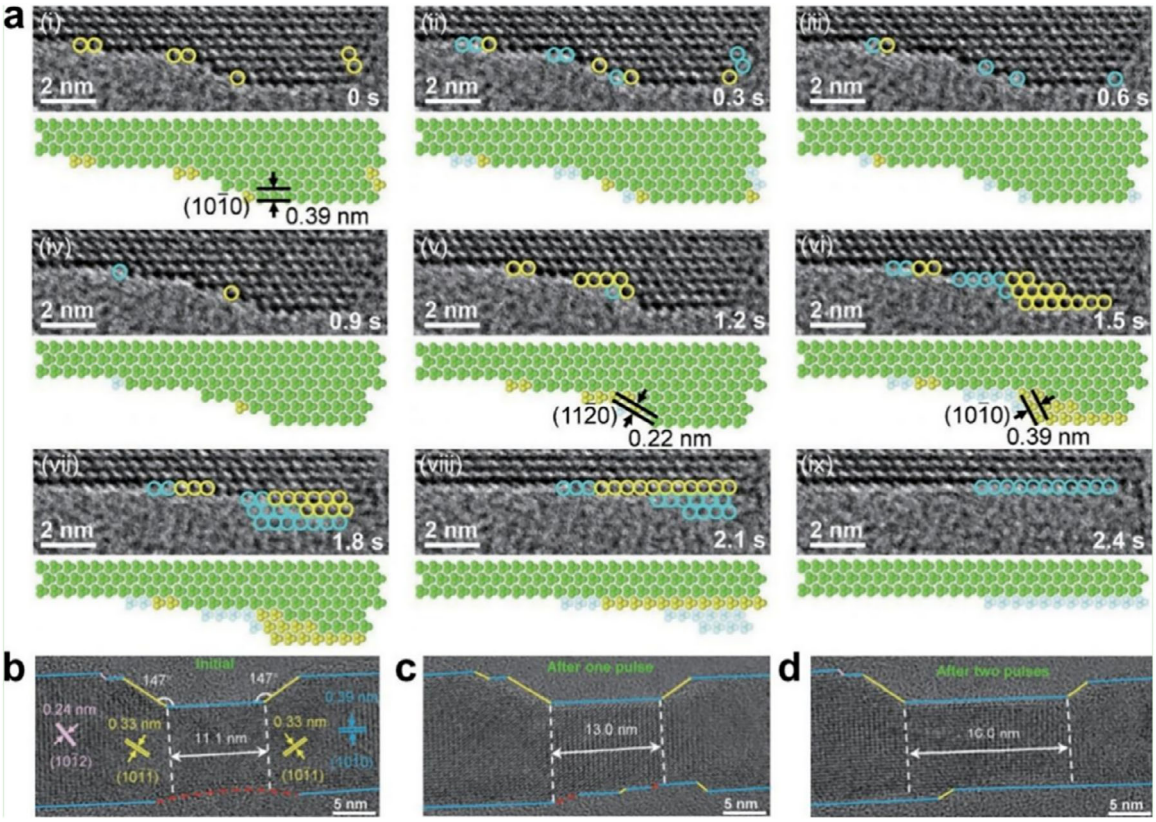

Figure 9. Atomic-scale sublimation under thermal excitation.[141] a) TEM images with corresponding schematic illustrations displaying the atomic sublimation. Yellow circles mark atomic chains undergoing sublimation in subsequent frames, while cyan circles identify atoms that have already sublimated compared to prior frames. b–d) TEM images of a Te nanowire before and after single-thermal-pulse and double-thermal-pulse treatments, respectively. Reproduced with permission.[141] Copyright 2022, Tsinghua University Press.

Recent advances have demonstrated electron-beam-mediated synthesis of metals and metal oxides in liquid environments. For example, Wei et al. achieved layer-by-layer growth of tetragonal Pb_3O_4 nanocrystals through electron beam-induced reduction of Pb^{2+} precursors within a thin liquid layer confined between carbon-film-coated TEM grids (**Figure 12**).[152] Dynamic observations revealed that the Pb_3O_4 nanocrystals initially grew along the [220] direction before transitioning to [002] as the [220] growth rate decreased, ultimately forming a well-defined tetragonal crystal. Image analysis reveals that the atomically rough surface along [220] promotes rapid nucleation, accounting for the preferential growth orientation. Similarly, reduction of H_2PtCl_6 precursors to Pt nanocrystals was achieved in LCTEM, with the growth rate increasing proportionally with electron beam dose.[153] In another study, controlled synthesis of metastable hexagonal close-packed (HCP) palladium hydride was realized by tuning the hydrogen-to-palladium ratio.[154] High H/ low Pd concentrations favored formation of the metastable HCP structure, whereas low H/ high Pd concentrations yielded the stable face-centered cubic structure.

Recent advances have enabled morphological control of nanomaterials, facilitating the synthesis of diverse nanostructures.[83,148,155–159] For example, Yang et al. demonstrated solution-phase transformation of transition metal oxides from 3D nanoparticles to 2D nanosheets by modulating reaction conditions under electron beam irradiation.[82] Such morphological evolution follows a size-dependent mechanism, once the particle exceeds a critical dimension, the increasing dominance of negative surface energy drives the transition from 3D to 2D configurations.[82]

Furthermore, another growth pathway, oriented attachment (OA), has also been directly visualized using LCTEM. Zhu et al. dynamically observed ligand-controlled OA behavior of Au nanoparticles.[85] When the center-to-center distance between two nanoparticles decreased below approximately twice the length of a ligand molecule ($L_{citrate}$), surface ligands began to overlap, initiating directional rotation of the nanoparticles (**Figure 13**). Real-time observations revealed that OA occurred along the {111} surfaces. As the interparticle separation approached ≈0.7 nm (comparable to $L_{citrate}$), the nanoparticles underwent OA through transient jump-to-contact events. Throughout this process, citrate ligands played a crucial role by modulating the interaction potential and introducing anisotropy into the binding energy landscape, thereby favoring attachment along specific crystal facets.

Additionally, integrating an electric bias into LCTEM establishes an electrochemical reaction platform, enabling atomic-scale manipulation and real-time visualization of electrochemical processes.[160–163] These investigations provide fundamental insights into the structural design and performance optimization of battery systems. Furthermore, the application of

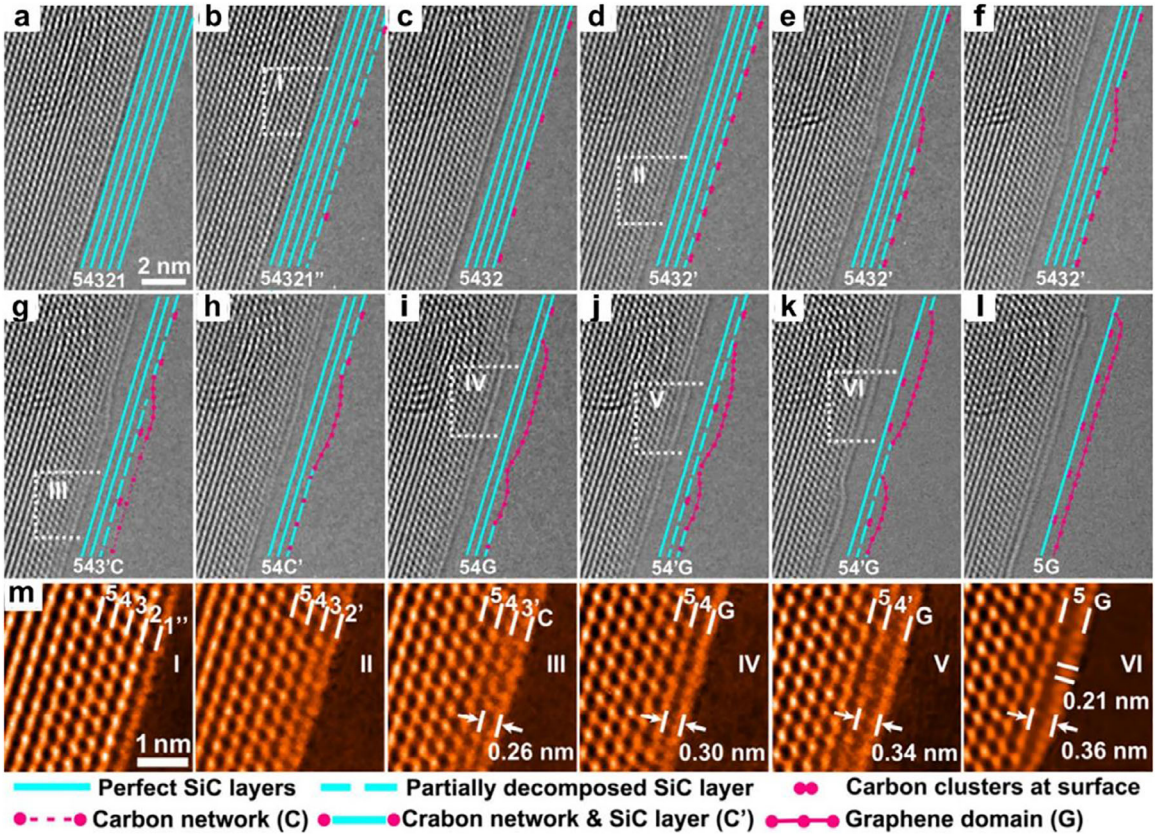

Figure 10. Formation of a graphene layer on the SiC(1$\bar{1}$00) surface at high temperature.[145] a–l) TEM images and corresponding schematic illustrations showing the stepwise growth of graphene on the SiC surface at 1000 °C. (m) Enlarged images of regions outlined by dashed rectangles, revealing detailed structures. Perfect SiC layers are indicated by 1, 2, 3, 4, and 5, while partially decomposed SiC layers are labeled 1′′, 2′, 3′, 4′. Reproduced with permission.[145] Copyright 2018, Tsinghua University Press and Springer–Verlag GmbH Germany.

electrical signals in LCTEM enables atomic-scale examination of electrified solid–liquid interfaces, elucidating surface reconstruction dynamics during electrocatalysis. For example, Zhang et al. employed a high-resolution electrochemical polymer liquid cell to visualize Cu-based CO_2 electroreduction, inducing surface atomic reconstruction on Cu catalysts.[163] **Figure 14**a illustrates a Cu nanowire connected to a Pt electrode, establishing an operando electrochemical system. Upon application of an external voltage, an amorphous interphase gradually forms on the Cu surface, exhibiting structural and contrast differences from the underlying crystalline Cu (Figure 14b,c). Real-time observations reveal a reversible transformation between amorphous and crystalline Cu phases, accompanied by atomic reorganization and dissolution (Figure 14d). HRTEM imaging elucidates atomic migration pathways at the three-phase boundary and amorphous–crystalline interface (Figure 14e,f), where Cu atoms detach from the crystalline region (yellow dashed line), migrate, and incorporate into the amorphous interphase. This dynamic process is driven by the formation and dissociation of unstable complexes (e.g., $[CuCO]^+$) and the electrochemical reduction of Cu^{2+} species. These results provide insights into atomic-scale surface reconstruction and enable precise control over catalytic performance.

3.5. Atomic-Scale Manufacturing in Gas Environment

The visualization of atomic-scale fabrication in gaseous environment is achieved using ETEM or gas-cell TEM, where fabrication can be precisely controlled by adjusting parameters such as gas composition, flow rate, and pressure.

Considerable efforts have been devoted to understanding the nucleation and growth of crystals in gaseous environments. For instance, Dick et al. achieved independent control over the nucleation and layer-by-layer growth processes of GaAs nanowires, as shown in **Figure 15**a,b.[164] Figure 15c schematically illustrates these nucleation and growth processes. Variations in Ga and As concentrations within the catalyst droplet, shown in Figure 15d, indicates that a continuous increase in Ga concentration enhances nucleation probability, while rapid depletion of As atoms prevents the formation of a complete monolayer, suggesting that layer growth is primarily governed by As concentration. By adjusting the partial pressures of the Ga and As precursors, researchers were able to regulate key properties of the nanowires, including composition, uniformity, and crystal structure. In another study, Chou et al. demonstrated that varying the growth temperature under reactive gases can alter the growth pathway of Si/Ge nanowires, thereby enabling the formation of

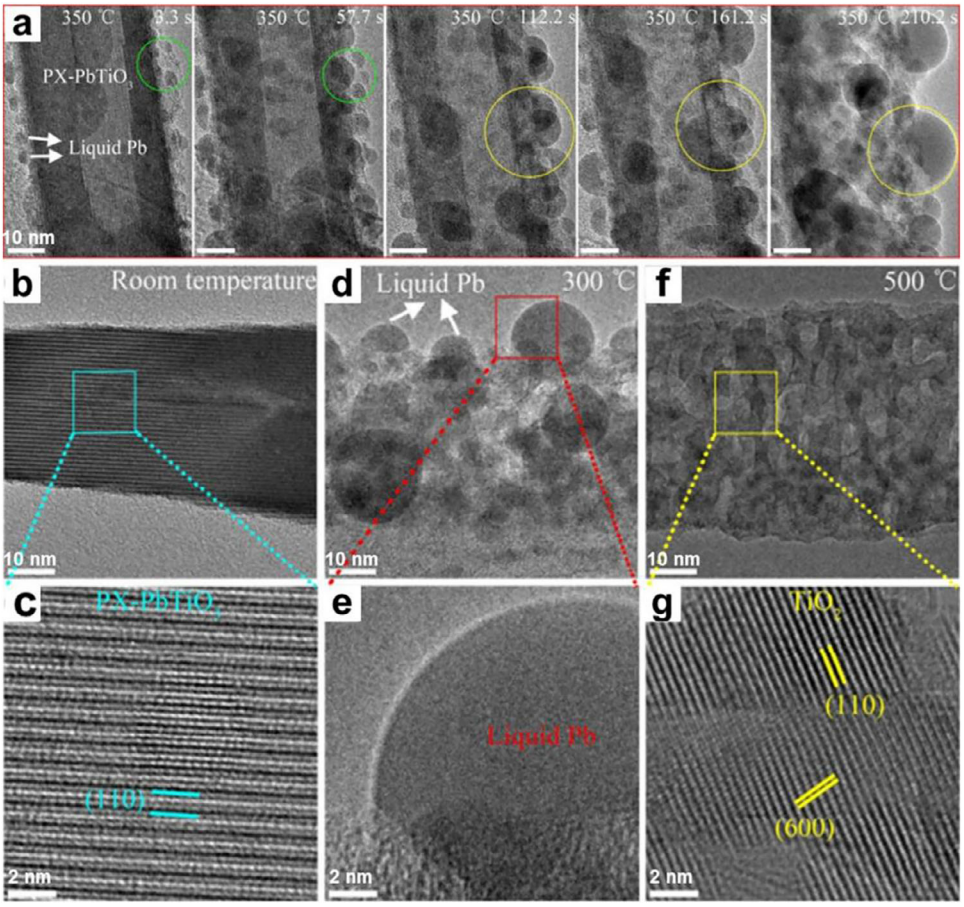

Figure 11. Thermally driven decomposition of PX-$PbTiO_3$ nanowires.[34] a) Growth of liquid Pb nanoparticles on the nanowire surface at 350 °C. b–g) TEM images of a nanowire during heat treatment at different temperature. (c), (e), and (g) show the corresponding HRTEM images of (b), (d), and (f), respectively. Reproduced with permission.[34] Copyright 2020, Tsinghua University Press and Springer-Verlag GmbH Germany.

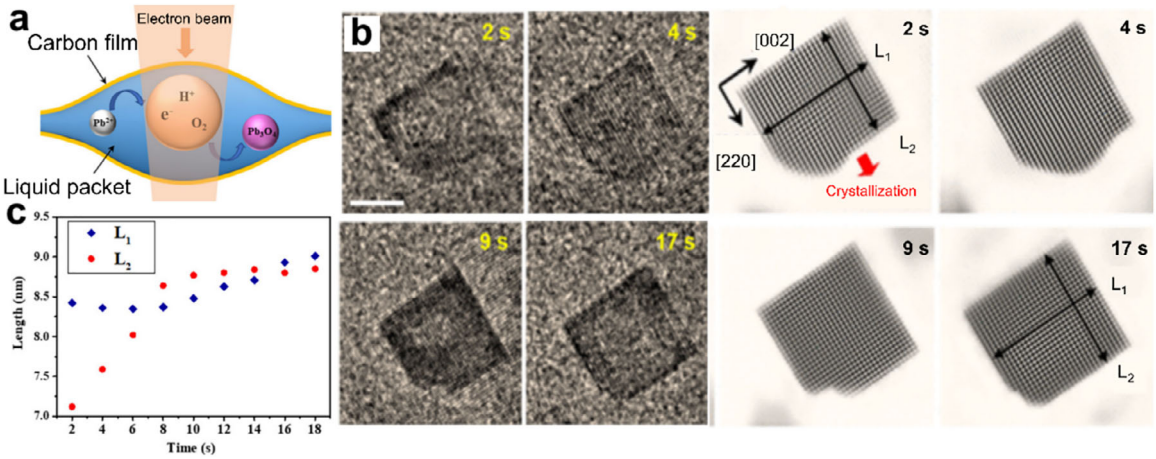

Figure 12. Growth of Pb_3O_4 nanocrystals in solution.[152] a) Schematic illustration of the experimental setup. b) Sequential TEM images and corresponding filtered images showing the monomer growth of a Pb_3O_4 nanocrystal. Scale bar: 5 nm. c) Size evolution of the Pb_3O_4 nanocrystal, where L_1 and L_2 denote the crystal lengths along the [002] and [220] directions, respectively. Reproduced with permission.[152] Copyright 2019, American Chemical Society.

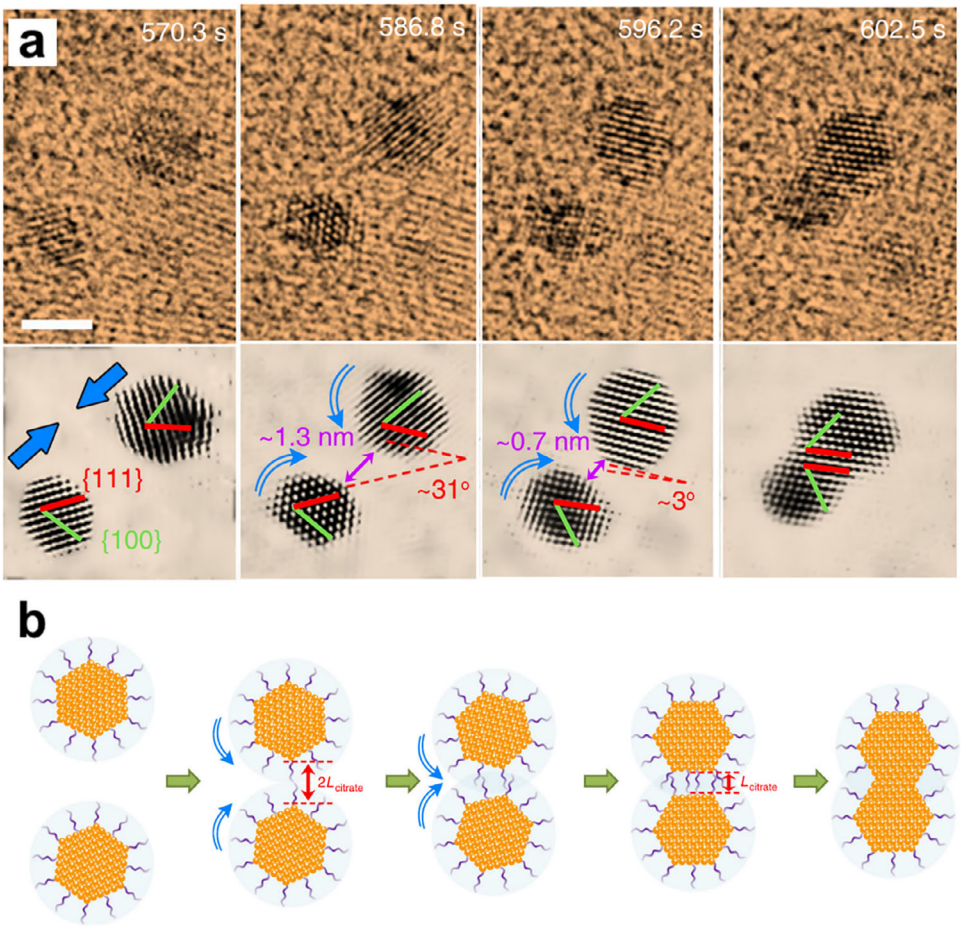

Figure 13. OA behavior of Au nanoparticles.[85] a) Atomic-resolution imaging of the OA process on the {111}surface. Scale bar: 2 nm. b) Schematic illumination of the OA process. Reproduced with permission.[85] Copyright 2018, The Author(s), Published by Springer Nature.

heterostructures with distinct properties.[165] Furthermore, catalyst-assisted growth of carbon nanotubes using gas-cell TEM has attracted considerable attention, as different catalysts markedly affect the growth pathway, growth rate, and crystallographic structure of the nanotubes.[166–168] Significant progress has also been made in the growth of two-dimensional structures, such as graphene films, under gaseous conditions.[169]

Tuning the gas environment enables precise control over nanocrystal morphology.[170–172] For example, Jiang et al. induced morphological evolution of PdCu nanocrystals by introducing a hydrogen atmosphere, as shown in **Figure 16**a,b.[173] When spherical PdCu nanocrystals supported on a SiN membrane were exposed to 1 bar of H_2 and annealed at 600 K, they transformed into truncated cubes with well-defined {001} and {011} facets. In contrast, PdCu nanocrystals annealed at 600 K under high-vacuum conditions (10^{-7} bar) retained their original spherical morphology. Density functional theory calculations revealed that hydrogen adsorption modifies the surface energy landscape (Figure 16c), facilitating surface atom diffusion. In another study, Zhang et al. carried out a morphology-controlled reshaping process, converting initially spherical Pd nanoparticles into faceted truncated-cube structures under 1 bar of N_2 at 200 °C.[174]

Phase modifications can also be triggered and visualized.[175–177] A classical example is reported by Dionne et al., that the α–β phase transition of Pd nanoparticles is controlled by varying H_2 pressure.[178,179] Zhang et al. reported a reversible structural modulation between a relaxed core–shell configuration and an alloyed phase during CO_2 hydrogenation.[180]

4. Conclusion and Outlook

Visualized atomic-scale manufacturing aims to achieve fabrication with atomic precision while simultaneously enabling real-time observation of dynamic structural evolution. Recent progress has been made through the integration of TEM with various external stimuli and environmental controls. Systematic investigations of electron beam irradiation effects, combined with advances in in situ techniques, have yielded critical insights into energy-matter interactions during fabrication and facilitated precise control over experimental parameters. On these foundations, TEM has progressively performed operations such as atomic etching, reconstruction, and growth, paving the way for the controlled fabrication of structures with atomic-scale features.

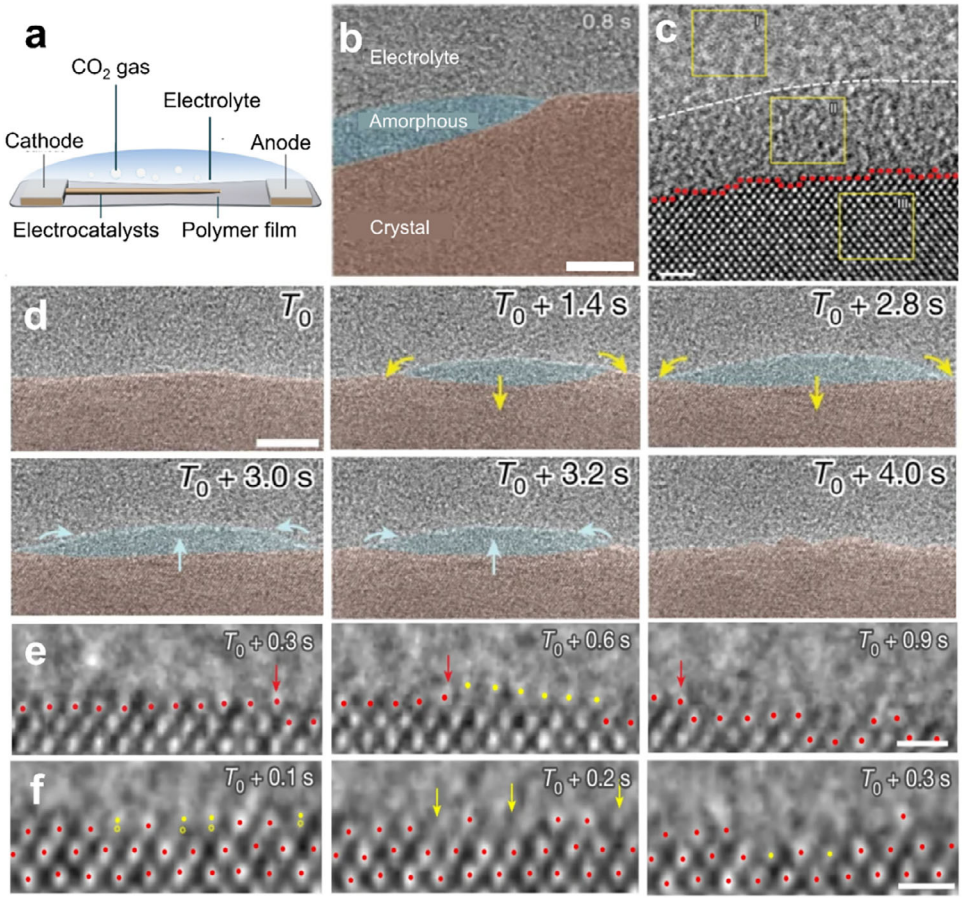

Figure 14. Construction of charged solid–liquid interfaces.[163] a) Schematic illustration of the sample region inside a polymer-based electrochemical liquid cell. b) TEM image revealing the emergence of an amorphous interphase during electrochemical operation. Scale bar: 5 nm. c) HRTEM image highlighting structural and contrast differences among the amorphous interphase, crystalline Cu, and the surrounding electrolyte. Scale bar: 1 nm. d) Time-series HRTEM images capturing the fluid-like dynamics and morphological evolution of the amorphous interphase (blue) between the solid catalyst (brown) and liquid electrolyte (gray) during electrochemical reduction. Scale bar: 5 nm. e) HRTEM image showing atomic-step-dependent behavior of Cu atoms at the triple-phase boundary. Scale bar: 5 nm. f) HRTEM image depicting random detachment of Cu atoms at the triple-phase boundary. Scale bar: 5 nm. Reproduced with permission.[163] Copyright 2024, Springer Nature.

Despite its substantially enhanced capabilities for atomic manipulation and its exceptional performance in atomic-scale manufacturing research, in situ TEM still faces challenges. From a characterization perspective, a primary challenge lies in achieving atomic resolution observations under external field stimuli. For instance, thermal drift at elevated temperatures and electron beam scattering from observation windows of liquid cells can markedly compromise spatial resolution. Furthermore, the temporal resolution of current in situ TEM methodologies—generally confined to the millisecond-to-microsecond regime—remains inadequate for capturing the rapid atomic-scale dynamics, such as atomic diffusion and chemical bond cleavage. An additional challenge arises from the pronounced discrepancy between the internal environment of TEM and practical fabrication conditions. In practical processes, materials are frequently exposed to ambient atmospheres rather than high vacuum, and chemical processes in liquid environments typically proceed in the absence of electron beam irradiation. More importantly, although numerous experimental achievements have been reported, systematic investigations and statistical analysis concerning the manufacturing processes within TEM remain scarce. While some efforts have been made to summarize processing conditions for specific structures,[125] the fundamental principles and intrinsic correlations across different material systems remain insufficiently understood. This gap underscores the urgent need to establish comprehensive databases that correlate processing parameters with material systems and target structures, thereby enabling more predictive and standardized manufacturing protocols. Additionally, the inherently low throughput of TEM-based atomic-scale manufacturing represents significant barriers to its industrial implementation and scale-up production.[181]

To address these challenges and further advance high-precision fabrication within TEM, several strategic directions are expected to guide future developments. First, the integration of advanced imaging techniques—such as ptychography and atomic electron tomography[182–184]—with multi-field coupling offers significant potential for extracting multi-attribute information from dynamic observations, thereby providing a more comprehensive understanding of complex manufacturing

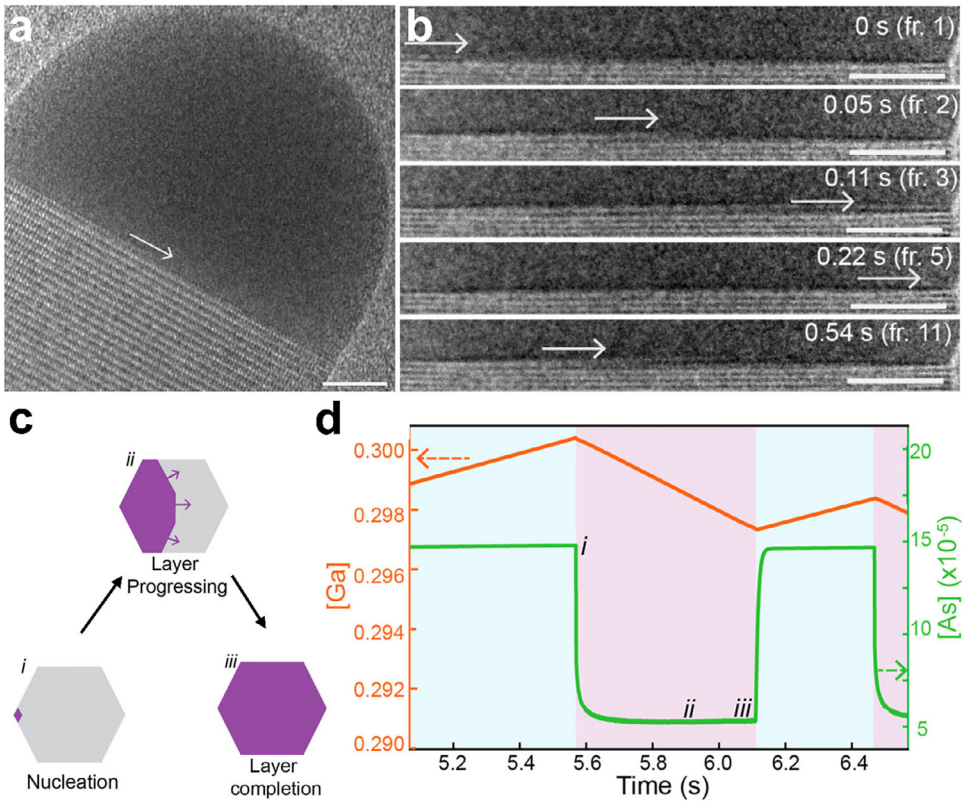

Figure 15. Gas-controlled nucleation and growth in nanowires.[164] a) TEM image of a GaAs NW during growth, along with its catalyst particle. A partially formed layer is visible (arrow). Scale bar: 5 nm. b) Sequential cropped frames from a video recording of another NW, illustrating the layer growth process. The frame number (fr.) and elapsed time relative to the first image are shown at the upper right of each panel. Scale bar: 5 nm. c) A schematic diagram illustrating the evolution of different stages of layer growth (nucleation, progressing and completion of a layer). d) Simulated evolution of Ga and As concentrations in the Au–Ga–As catalyst droplet over time. The collection and depletion of Ga proceed more slowly than those of As, while the As concentration remains several orders of magnitude lower. The stages of layer growth—nucleation, progression, and completion—are indicated as (i), (ii), and (iii), respectively. Reproduced with permission.[164] Copyright 2020, American Chemical Society.

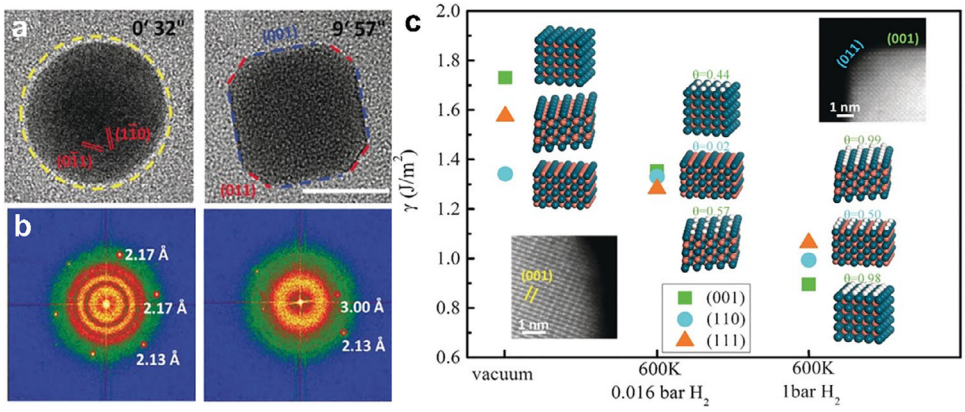

Figure 16. Morphology regulation of PdCu nanocrystals.[173] a) Lattice-resolved TEM images and b) corresponding FFT patterns showing the morphological evolution of PdCu nanocrystals upon exposure to H_2 at 1 bar and heating to 600 K. Scale bar: 10 nm. c) Surface energies and structural models of the (001), (110) and (111) surfaces. Pd atoms are depicted in blue, Cu atoms in orange and H atoms in white. Insets show high-angle annular dark field images of these surfaces for spherical and surface-faceted PdCu nanocrystals. Reproduced with permission.[173] Copyright 2016, WILEY-VCH.

processes. Second, deep learning and artificial intelligence are expected to play pivotal roles in automating electron-beam trajectory planning, optimizing process parameters through historical data analysis, and processing large data streams from in situ TEM, ultimately establishing closed-loop feedback systems for atomic-scale manufacturing. In addition, advanced algorithms can support drift compensation, environmental monitoring, and real-time correction to mitigate the effects of atomic-scale drift and environmental fluctuations. These advances will be critical for improving the stability, precision, and efficiency of manufacturing processes at the atomic scale. Finally, additional promising avenues include the development of parallel processing strategies to enhance throughput, the integration of TEM with complementary platforms such as atomic force microscopy, and the refinement of models to more effectively bridge experimental observation with practical manufacturing.

Acknowledgements

M.Z. and C.L. contributed equally to this work. This work was supported by the National Key R&D Program of China (No. 2022YFB4400100), the National Natural Science Foundation of China (Nos. 12234005, T2321002), the Key R&D Program of Jiangsu Province (No. BE2023009-4), New Cornerstone Science Foundation.

Conflict of Interest

The authors declare no conflict of interest.

Data Availability Statement

The data that support the findings of this study are available in the supplementary material of this article

Keywords

atomic-scale manufacturing, dynamical visualization, electron beam machining, in situ transmission electron microscopy, process mechanism

Received: October 9, 2025
Revised: November 17, 2025
Published online: December 26, 2025

[1] X. Cheng, Z. Pan, C. Fan, Z. Wu, Li Ding, L.-M. Peng, *Sci. Adv.* **2024**, *10*, adl1636.
[2] P. Soothar, H. Wang, C. Xu, Yu Quan, Z. A. Dayo, M. Aamir, B. Muneer, *Int. J. Antennas Propag.* **2021**, *2021*, 9912008.
[3] H. Yu, Y. Chong, P. Zhang, J. Ma, D. Li, *Talanta* **2020**, *219*, 121324.
[4] S. Zhao, J. Zhang, L. Fu, *Adv. Mater.* **2021**, *33*, 2005544.
[5] J. Gao, X. Luo, F. Fang, J. Sun, *Int. J. Extrem. Manuf.* **2021**, *4*, 1.
[6] E. Bussmann, R. E. Butera, J. H. G. Owen, J. N. Randall, S. M. Rinaldi, A. D. Baczewski, S. Misra, *MRS Bull.* **2021**, *46*, 607.
[7] A. M. Jakob, S. G. Robson, H. R. Firgau, V. Mourik, V. Schmitt, D. Holmes, M. Posselt, E. L. H. Mayes, D. Spemann, J. C. McCallum, A. Morello, D. N. Jamieson, *Adv. Mater.* **2024**, *36*, 2405006.
[8] A. D. Tranter, L. Kranz, S. Sutherland, J. G. Keizer, S. K. Gorman, B. C. Buchler, M. Y. Simmons, *ACS Nano* **2024**, *18*, 19489.
[9] T. Esat, D. Borodin, J. Oh, A. J. Heinrich, F. S Tautz, Y. Bae, R. Temirov, *Nat. Nanotechnol.* **2024**, *19*, 1466.
[10] R. Li, W. Guo, Z. Zhu, Y. Zhai, G. Wang, Z. Liu, L. Jiao, C. Zhu, X. Lu, *Anal. Chem.* **2023**, *95*, 7195.
[11] X. Chen, Y. Zhou, V. A. L. Roy, S.-T. Han, *Adv. Mater.* **2018**, *30*, 1703950.
[12] F. E. Kalff, M. P. Rebergen, E. Fahrenfort, J. Girovsky, R. Toskovic, J. L. Lado, J. Fernández-Rossier, A. F. Otte, *Nat. Nanotechnol.* **2016**, *11*, 926.
[13] Y. Shang, X. Li, J. Song, S. Huang, Z. Yang, Z. J. Xu, H. Y. Yang, *Chem* **2020**, *6*, 1804.
[14] J. Sun, M. Sadd, P. Edenborg, H. Grönbeck, P. H. Thiesen, Z. Xia, V. Quintano, R. Qiu, A. Matic, V. Palermo, *Sci. Adv.* **2021**, *7*, abf0812.
[15] Y. Zeng, B. Ouyang, J. Liu, Y.-W. Byeon, Z. Cai, L J. Miara, Y. Wang, G. Ceder, *Science* **2022**, *378*, 1320.
[16] M. Fuechsle, J. A. Miwa, S. Mahapatra, H. Ryu, S. Lee, O. Warschkow, L. C. L. Hollenberg, G. Klimeck, M. Y. Simmons, *Nat. Nanotechnol.* **2012**, *7*, 242.
[17] J. Wyrick, X. Wang, R V. Kashid, P. Namboodiri, S W. Schmucker, J A. Hagmann, K. Liu, M D. Stewart, C A. Richter, G W. Bryant, R M. Silver, *Adv. Funct. Mater.* **2019**, *29*, 1903475.
[18] L. Ma, X. Lei, J. Yan, R. Li, T. Chai, Z. Yan, X. Jia, C. Xie, K. Pen, *Nat. Commun.* **2022**, *13*, 2368.
[19] H. Yu, S. J. Kim, J. B. Kim, *J. Korean Phys. Soc.* **2023**, *82*, 819.
[20] T. Sato, N. Nishimura, N. Kaku, S. Otabe, T. Kawasaki, T. Hosoya, M. Kozuma, *Phys. Rev. Appl.* **2025**, *23*, 044001.
[21] Y. Han, L. Wang, Ke Cao, J. Zhou, Y. Zhu, Y. Hou, Y. Lu, *Chem. Rev.* **2023**, *123*, 14119.
[22] B. Kiraly, E. J. Knol, W. M. J. van Weerdenburg, H. J. Kappen, A. A. Khajetoorians, *Nat. Nanotechnol.* **2021**, *16*, 414.
[23] S. T. Howell, A. Grushina, F. Holzner, J. Brugger, *Microsyst. Nanoeng.* **2020**, *6*, 21.
[24] F. Rahman, J. C. Runyon, *IEEE Tran. on Semicond. Manuf.* **2021**, *34*, 500.
[25] V. R. Manfrinato, L. Zhang, D. Su, H. Duan, R. G. Hobbs, E. A. Stach, K. K. Berggren, *Nano Lett.* **2013**, *13*, 1555.
[26] F. E. Camino, V. R. Manfrinato, A. Stein, L. Zhang, M. Lu, E. A. Stach, C. T. Black, *J. Vis. Exp.* **2018**, *139*, 58272.
[27] X. Liu, T. Xu, X. Wu, Z. Zhang, J. Yu, H. Qiu, J.-H. Hong, C.-H. Jin, J.-X. Li, X.-R. Wang, L.-T. Sun, W. Guo, *Nat. Commun.* **2013**, *4*, 1776.
[28] K. Yin, Y.-Y. Zhang, Y. Zhou, L. Sun, M. F. Chisholm, S. T. Pantelides, W. Zhou, *2D Mater.* **2017**, *4*, 011001.
[29] Y. Zhu, W. Ai, M. Ye, C. Li, M. Zhou, F. Chu, G. Dong, Y. Zhou, X. Hu, T. Xu, L. Sun, *Nano Today* **2024**, *59*, 102540.
[30] Y. Shen, T. Xu, X. Tan, L. He, K. Yin, N. Wan, L. Sun, *Adv. Mater.* **2018**, *30*, 1705954.
[31] J. Haas, F. Ulrich, C. Hofer, X. Wang, K. Braun, J C. Meyer, *ACS Nano* **2022**, *16*, 1836.
[32] R. F. Egerton, P. Li, M. Malac, *Micron* **2004**, *35*, 399.
[33] X. Han, M. Niu, Y. Luo, R. Li, J. Dan, Y. Hong, Xu Wu, A V. Trukhanov, W. Ji, Y. Wang, J. Zhou, J. Qiao, J. Zhang, X. Zhao, *Nat. Synth.* **2024**, *3*, 586.
[34] H. Zhang, W. Wang, T. Xu, F. Xu, L. Sun, *Nano Res.* **2020**, *13*, 1912.
[35] E. Sutter, Y. Huang, H.-P. Komsa, M. Ghorbani-Asl, A. V. Krasheninnikov, P. Sutter, *Nano Lett.* **2016**, *16*, 4410.
[36] T. Xu, X. Xie, K. Yin, J. Sun, L. He, L. Sun, *Small* **2014**, *10*, 1724.
[37] K M. Roccapriore, M G. Boebinger, O. Dyck, A. Ghosh, R R. Unocic, S V. Kalinin, M. Ziatdinov, *ACS Nano* **2022**, *16*, 17116.
[38] F. Zheng, D. Guo, L. Huang, L. W. Wong, X. Chen, C. Wang, Y. Cai, N. Wang, C.-S. Lee, S. P. Lau, T. H. Ly, W. Ji, J. Zhao, *Adv. Sci.* **2022**, *9*, 2200702.
[39] O. Dyck, S. Kim, S. V. Kalinin, S. Jesse, *Nano Res.* **2018**, *11*, 6217.
[40] O. Dyck, A. R. Lupini, S. Jesse, *Nano Lett.* **2023**, *23*, 2339.
[41] Y. Liu, X. Chen, K. W. Noh, S. J. Dillon, *Nanotechnology* **2012**, *23*, 385302.

[42] T. Noriki, S. Abe, K. Kajikawa, M. Shimojo, *Beilstein J. Nanotechnol.* **2015**, *6*, 1010.
[43] Q. Cheek, E. Fahrenkrug, S. Hlynchuk, D. H. Alsem, N J. Salmon, S. Maldonado, *ACS Nano* **2020**, *14*, 2869.
[44] D. Alloyeau, W. Dachraoui, Y. Javed, H. Belkahla, G. Wang, H. Lecoq, S. Ammar, O. Ersen, A. Wisnet, F. Gazeau, C. Ricolleau, *Nano Lett.* **2015**, *15*, 2574.
[45] W. Xia, Q. An, L. Chen, R. Cai, *Micron* **2024**, *181*, 103622.
[46] H. Sheng, He Zheng, S. Jia, M K. Y. Chan, T. Rajh, J. Wang, J. Wen, *Nanoscale* **2019**, *11*, 10756.
[47] H. Zhang, T. Xu, Y. Zhu, W. Wang, H. Zhang, D. Yuan, L. Sun, *Nanomaterials* **2021**, *11*, 1021.
[48] S. Peng, L. Xu, Z. Cao, C. Jiao, W. Liu, Y. Lu, W. Wang, B. Chen, *Nano Lett.* **2025**, *25*, 3662.
[49] O. Dyck, S. Yeom, A. R. Lupini, J. L. Swett, D. Hensley, M. Yoon, S. Jesse, *Adv. Mater.* **2023**, *35*, 2302906.
[50] O. Dyck, S. Jesse, N. Delby, S. V. Kalinin, A. R. Lupini, *Ultramicroscopy* **2020**, *211*, 112949.
[51] S. Kretschmer, T. Lehnert, U. Kaiser, A. V. Krasheninnikov, *Nano Lett.* **2020**, *20*, 2865.
[52] S. de Graaf, B. J. Kooi, *2D Mater.* **2022**, *9*, 015009.
[53] Y. Zhang, C. Wang, X. Wu, *Nanoscale* **2022**, *14*, 9542.
[54] P. Nukala, M. Ahmadi, Y. Wei, S. de Graaf, E. Stylianidis, T. Chakrabortty, S. Matzen, H W. Zandbergen, A. Björling, D. Mannix, D. Carbone, B. Kooi, B. Noheda, *Science* **2021**, *372*, 630.
[55] H. Bai, X. Su, D. Yang, Q. Zhang, G. Tan, C. Uher, X. Tang, J. Wu, *Adv. Funct. Mater.* **2021**, *31*, 2100431.
[56] Qi Liang, D. Yang, F. Xia, H. Bai, H. Peng, R. Yu, Y. Yan, D. He, S. Cao, G. Van Tendeloo, G. Li, Q. Zhang, X. Tang, J. Wu, *Adv. Funct. Mater.* **2021**, *31*, 2106938.
[57] H. Ye, Z. Zhang, R. Wang, *Small* **2023**, *19*, 2303872.
[58] D. S. Gavhane, A. D. Sontakke, M. A. van Huis, *Adv. Funct. Mater.* **2022**, *32*, 2106450.
[59] F. Cheng, L. Lian, L. Li, J. Rao, C. Li, T. Qi, Y. Cheng, Z. Zhang, J. Zhang, J. Wang, Y. Gao, *Nano Energy* **2020**, *75*, 104816.
[60] J. Li, Z. Wang, Y. Li, F. L. Deepak, *Adv. Sci.* **2019**, *6*, 1802131.
[61] C. Luo, J. Li, X. Yang, X. Wu, S. Zhong, C. Wang, L. Sun, *ACS Appl. Nano Mater.* **2020**, *3*, 4747.
[62] S. Sheng, T. Wang, S. Liu, F. Liu, B. Sheng, Y. Yuan, D. Li, Z. Chen, R. Tao, L. Chen, B. Zhang, J. Yang, P. Wang, D. Wang, X. Sun, J. Zhang, J. Xu, W. Ge, B. Shen, X. Wang, *Adv. Sci.* **2022**, *9*, 2106028.
[63] L. Tang, W. Wu, L. He, T. Xu, H. Dong, L. Zhang, L. Shi, L. Sun, *J. Alloys Compd.* **2021**, *877*, 160168.
[64] C. Qiu, L. Schaffer, M. Li, M. Paulose, J. Tam, S. Chen, P K S. Nonis, A. Lim, J Y. Howe, O K. Varghese, *Mater. Today Nano* **2025**, *31*, 100654.
[65] X. Fu, Xu-D Wang, B. Zhao, Q. Zhang, S. Sun, J.-J. Wang, W. Zhang, L. Gu, Y. Zhang, W.-Z. Zhang, W. Wen, Ze Zhang, L.-Q. Chen, Q. Yu, En Ma, *Nat. Mater.* **2022**, *21*, 290.
[66] I. Cora, Zs. Fogarassy, R. Fornari, M. Bosi, A. Recnik, B. Pécz, *Acta Mater.* **2020**, *183*, 216.
[67] C. Luo, Z. Dong, T. Xu, X. Yang, H. Zhang, H. Bi, C. Wang, L. Sun, J. Chu, X. Wu, *Nanoscale* **2022**, *14*, 16077.
[68] T. W. Hansen, J. B. Wagner, R. E. Dunin-Borkowski, *Mater. Sci. Technol.* **2010**, *26*, 1338.
[69] L. L. Dai, R. Sharma, C.-y. Wu, *Langmuir* **2005**, *21*, 2641.
[70] A. N. Bright, K. Yoshida, N. Tanaka, *Ultramicroscopy* **2013**, *124*, 46.
[71] K. Kishita, H. Sakai, H. Tanaka, H. Saka, K. Kuroda, M. Sakamoto, A. Watabe, T. Kamino, *J. Electron Microsc.* **2009**, *58*, 331.
[72] J Yu Huang, Li Zhong, C. M. Wang, J P. Sullivan, Wu Xu, Li Q Zhang, S X. Mao, N S. Hudak, X. H. Liu, A. Subramanian, H. Fan, L. Qi, A. Kushima, Ju Li, *Science* **2010**, *330*, 1515.
[73] S. Lee, Y. Oshima, E. Hosono, H. Zhou, K. Kim, H M. Chang, R. Kanno, K. Takayanagi, *J. Phys. Chem. C* **2013**, *117*, 24236.
[74] H. Lv, W. Si, J. Sha, Y. Chen, Y. Zhang, *Next Nanotechnol.* **2025**, *7*, 100115.
[75] Y. Chen, K. Yin, T. Xu, H. Guo, L. Sun, *ACS Appl. Nano Mater.* **2023**, *6*, 22545.
[76] T. Tarnawski, M. Parlińska-Wojtan, *Chem.–Methods* **2024**, *4*, 202300041.
[77] J. Zhang, Z. Sun, Z. Kang, H. Lin, H. Liu, Y. He, Z. Zeng, Q. Zhang, *Adv. Funct. Mater.* **2022**, *32*, 2204976.
[78] H. Zheng, *Isr. J. Chem.* **2025**, *65*, e202400061.
[79] H. Zheng, R K. Smith, Y.-W. Jun, C. Kisielowski, U. Dahmen, A. P Alivisatos, *Science* **2009**, *324*, 1309.
[80] S. Khalil, M. Sun, Z. Yang, A. B. Marciel, M. R. Jones, R. Verduzco, *Small* **2025**, *21*, 02087.
[81] W. Zheng, J. Kang, K. Niu, C. Ophus, E M. Chan, P. Ercius, L.-W. Wang, J. Wu, H. Zheng, *Sci. Adv.* **2024**, *10*, adn6426.
[82] J. Yang, Z. Zeng, J. Kang, S. Betzler, C. Czarnik, X. Zhang, C. Ophus, C. Yu, K. Bustillo, M. Pan, J. Qiu, L.-W. Wang, H. Zheng, *Nat. Mater.* **2019**, *18*, 970.
[83] H.-G. Liao, L. Cui, S. Whitelam, H. Zheng, *Science* **2012**, *336*, 1011.
[84] X. Peng, J. Shangguan, Q. Zhang, M. Hauwiller, H. Yu, Y. Nie, K C. Bustillo, A. P Alivisatos, M. Asta, H. Zheng, *Nano Lett.* **2024**, *24*, 1168.
[85] C. Zhu, S. Liang, E. Song, Y. Zhou, W. Wang, F. Shan, Y. Shi, C. Hao, K. Yin, T. Zhang, J. Liu, H. Zheng, L. Sun, *Nat. Commun.* **2018**, *9*, 421.
[86] W. Wang, T. Xu, T. Bai, C. Zhu, Q. Zhang, H. Zhang, H. Zhang, Z. Guo, H. Zheng, L. Sun, *Sci. China Mater.* **2020**, *63*, 2599.
[87] M. Ye, T. Xu, Y. Xiong, Y. Zhu, M. Zhou, L. Han, J. Sun, M. Qin, L. Sun, *Nano Res.* **2024**, *17*, 7786.
[88] J. Park, K. Koo, N. Noh, J Ha Chang, J. Y. Cheong, K. S. Dae, Ji Su Park, S. Ji, Il-D Kim, J. M. Yuk, *ACS Nano* **2021**, *15*, 288.
[89] J. M. Yuk, J. Park, P. Ercius, K. Kim, D J. Hellebusch, M F. Crommie, J. Y. Lee, A. Zettl, A. P Alivisatos, *Science* **2012**, *336*, 61.
[90] N. Clark, D J. Kelly, M. Zhou, Yi-C Zou, C. W. Myung, D G. Hopkinson, C. Schran, A. Michaelides, R. Gorbachev, S J. Haigh, *Nature* **2022**, *609*, 942.
[91] J. Yang, M. K. Choi, Y. Sheng, J. Jung, K. Bustillo, T. Chen, S.-W. Lee, P. Ercius, Ji H Kim, J H. Warner, E M. Chan, H. Zheng, *Nano Lett.* **2019**, *19*, 1788.
[92] Y. Zeng, Z. Zhang, H. Ye, H. Qiu, R. Wang, *J. Phys. D: Appl. Phys.* **2025**, *58*, 143003.
[93] L. Sun, F. Banhart, J. Warner, *MRS Bull.* **2015**, *40*, 29.
[94] H. Qiu, T. Xu, Z. Wang, W. Ren, H. Nan, Z. Ni, Q. Chen, S. Yuan, F. Miao, F. Song, G. Long, Yi Shi, L. Sun, J. Wang, X. Wang, *Nat. Commun.* **2013**, *4*, 2642.
[95] T. Xu, Y. Tu, Y. Zhu, Y. Shen, K. Yin, L. Sun, *Nanoscale* **2022**, *14*, 17182.
[96] Y. Shen, T. Xu, X. Tan, J. Sun, L. He, K. Yin, Y. Zhou, F. Banhart, L. Sun, *Nano Lett.* **2017**, *17*, 5119.
[97] O. Dyck, A. R. Lupini, S. Jesse, *Small Methods* **2023**, *7*, 2300401.
[98] T An Bui, G T. Leuthner, J. Madsen, M R. A. Monazam, A I. Chirita, A. Postl, C. Mangler, J. Kotakoski, T. Susi, *Small* **2023**, *19*, 2301926.
[99] Y. Shen, H. Yu, T. Xu, Q. Zhang, K. Yin, S. Cong, Y. Liu, L. Sun, *Nano Res.* **2022**, *15*, 4710.
[100] M. G. Boebinger, D E. Yilmaz, A. Ghosh, S. Misra, T. S. Mathis, S. V. Kalinin, S. Jesse, Y. Gogotsi, A. C. T. van Duin, R R. Unocic, *Small Methods* **2024**, *8*, 2400203.
[101] M. G. Boebinger, C. Brea, L.-P. Ding, S. Misra, O. Olunloyo, Y. Yu, K. Xiao, A. R. Lupini, F. Ding, G. Hu, P. Ganesh, S. Jesse, R. R. Unocic, *Adv. Mater.* **2023**, *35*, 2210116.
[102] R. N. Keneipp, J. A. Gusdorff, P. Bhatia, T. T. Shin, L. C. Bassett, M. Drndic, *J. Phys. Chem. C* **2024**, *128*, 8741.
[103] H. Duan, X. Wang, T. Zheng, Y. Song, K. Du, *Adv. Funct. Mater.* **2025**, *35*, 2412694.

[104] J. Lin, O. Cretu, W. Zhou, K. Suenaga, D. Prasai, K. I. Bolotin, N. T. Cuong, M. Otani, S. Okada, A. R. Lupini, J.-C. Idrobo, D. Caudel, A. Burger, N. J. Ghimire, J. Yan, D. G. Mandrus, S. J. Pennycook, S. T. Pantelides, *Nat. Nanotechnol.* **2014**, *9*, 436.
[105] T. Xu, Y. Zhou, X. Tan, K. Yin, L. He, F. Banhart, L. Sun, *Adv. Funct. Mater.* **2017**, *27*, 1603897.
[106] R. Zan, Q. M. Ramasse, U. Bangert, K. S. Novoselov, *Nano Lett.* **2012**, *12*, 3936.
[107] G. Li, C. Zou, F. Wang, Z.-K. Han, W. Yuan, H. Yang, Y. Wang, *Adv. Funct. Mater.* **2024**, *34*, 2410524.
[108] J. Si, M. Zeng, H Q. Ta, S. Zheng, J. Liao, X. Yang, M H. Rümmeli, L. Fu, *Small* **2020**, *16*, 2001325.
[109] K. Yu, T. Xu, X. Wu, W. Wang, H. Zhang, Q. Zhang, L. Tang, L. Sun, *Research* **2019**, *2019*, 3289247.
[110] F. Börrnert, S. M. Avdoshenko, A. Bachmatiuk, I. Ibrahim, B. Büchner, G. Cuniberti, M. H. Rümmeli, *Adv. Mater.* **2012**, *24*, 5630.
[111] B. C. Bayer, R. Kaindl, M. Reza Ahmadpour Monazam, T. Susi, J. Kotakoski, T. Gupta, D. Eder, W. Waldhauser, J. C. Meyer, *ACS Nano* **2018**, *12*, 8758.
[112] S. Jesse, Q. He, A. R. Lupini, D. N. Leonard, M. P. Oxley, O. Ovchinnikov, R. R. Unocic, A. Tselev, M. Fuentes-Cabrera, B. G. Sumpter, S. J. Pennycook, S. V. Kalinin, A. Y. Borisevich, *Small* **2015**, *11*, 5895.
[113] D. Zangeneh, B. Sapkota, R. Uppuluri, R. F. Klie, *Chem. Mater.* **2025**, *37*, 1491.
[114] X. Huang, S. Li, Y. Huang, S. Wu, X. Zhou, S. Li, C. L. Gan, F. Boey, C. A. Mirkin, H. Zhang, *Nat. Commun.* **2011**, *2*, 292.
[115] S. B. Lee, J. Jung, H. N. Han, *Acta Mater.* **2023**, *247*, 118759.
[116] Y. Li, J. Xia, X. Li, L. Tian, P. Qiao, J. Cao, Z. Zhang, Q. Meng, J. Li, C. Liu, X. Meng, *Nano Today* **2024**, *59*, 102532.
[117] F. Saleem, X. Cui, Z. Zhang, Z. Liu, J. Dong, Bo Chen, Ye Chen, H. Cheng, X. Zhang, F. Ding, H. Zhang, *Small* **2019**, *15*, 1903253.
[118] Y.-C. Lin, D. O. Dumcenco, Y.-S. Huang, K. Suenaga, *Nat. Nanotechnol.* **2014**, *9*, 391.
[119] J. Lin, S. Zuluaga, P. Yu, Z. Liu, S. T. Pantelides, K. Suenaga, *Phys. Rev. Lett.* **2017**, *119*, 016101.
[120] T. Xu, H. Zhang, M. Ye, Y. Zhu, D. Yuan, W. Li, Y. Zhou, L. Sun, *Nanoscale* **2022**, *14*, 12569.
[121] S. Meng, J. Wu, L. Zhao, H. Zheng, S. Jia, S. Hu, W. Meng, S. Pu, D. Zhao, J. Wang, *Chem. Mater.* **2018**, *30*, 7306.
[122] J. Zhao, Q. Deng, A. Bachmatiuk, G. Sandeep, A. Popov, J. Eckert, M. H. Rümmeli, *Science* **2014**, *343*, 1228.
[123] H. Q. Ta, Q. X. Yang, S. Liu, A. Bachmatiuk, R. G. Mendes, T. Gemming, Y. Liu, L. Liu, K. Tokarska, R. B. Patel, J.-H. Choi, M. H. Rümmeli, *Nano Lett.* **2020**, *20*, 4354.
[124] R. G. Mendes, H. Q. Ta, T. Gemming, H. van Gog, M. A. van Huis, A. Bachmatiuk, M. H. Rümmeli, *Adv. Funct. Mater.* **2025**, *35*, 2412889.
[125] H. Q. Ta, R. G. Mendes, Y. Liu, X. Yang, J. Luo, A. Bachmatiuk, T. Gemming, M. Zeng, L. Fu, L. Liu, M. H. Rümmeli, *Adv. Sci.* **2021**, *8*, 2100619.
[126] Z. Qu, W. Zhang, S. Wang, D. Chen, Y. Yao, M. Cheng, L. Dong, *Adv. Sci.* **2025**, *12*, 2500553.
[127] J. M. Yuk, K. Kim, Z. Lee, M. Watanabe, A. Zettl, T. W. Kim, Y. S. No, W. K. Choi, J. Y. Lee, *ACS Nano* **2010**, *4*, 2999.
[128] H. Zhang, T. Xu, K. Yu, W. Wang, L. He, L. Sun, *Nat. Commun.* **2021**, *12*, 4812.
[129] F. Ma, K. A. Abboud, C. Zeng, *Nat. Synth.* **2023**, *2*, 949.
[130] R. Zeng, K. Lian, Bo Su, L. Lu, J. Lin, D. Tang, S. Lin, X. Wang, *Angew. Chem., Int. Ed.* **2021**, *60*, 25055.
[131] Q. Zhang, K. Yin, H. Dong, Y. Zhou, X. Tan, K. Yu, X. Hu, T. Xu, C. Zhu, W. Xia, F. Xu, H. Zheng, L. Sun, *Nat. Commun.* **2017**, *8*, 14889.
[132] S. Dai, C. Yang, Y. Wang, Y. Jiang, L. Zeng, *Adv. Sci.* **2025**, *12*, 2500513.
[133] Y. Hu, Y. Nian, M. Wang, N. Wang, Y. Qiu, L. Zhang, X. Li, Y. Han, L. Luo, *ACS Mater. Lett.* **2024**, *6*, 3335.
[134] G. Wang, Y. Zhang, H. S. Cho, X. Zhao, F. Kim, J. Zou, *ACS Appl. Energy Mater.* **2021**, *4*, 14180.
[135] M. Wang, S. Xu, J. J. Cha, *Adv. Energy Sustain. Res.* **2021**, *2*, 2100027.
[136] S. Sun, C. Liu, J. Liang, W. Wang, R. Li, L. Zhao, C. Dai, *ACS Nano* **2024**, *18*, 8283.
[137] M. Rajapakse, B. Karki, U. O. Abu, S. Pishgar, M. R. K. Musa, S. M. S. Riyadh, M. Yu, G. Sumanasekera, J. B. Jasinski, *npj 2D Mater. Appl.* **2021**, *5*, 30.
[138] W. Li, X. Qian, J. Li, *Nat. Rev. Mater.* **2021**, *6*, 829.
[139] S. Chen, L. Wang, R. Shao, J. Zou, R. Cai, J. Lin, C. Zhu, J. Zhang, F. Xu, J. Cao, J. Feng, J. Qi, P. Gao, *Nano Energy* **2018**, *48*, 560.
[140] R. Fu, Y. Pan, Y. Hua, L. Su, S. Hou, Y. Xiong, S.-Y. Lei, H. Min, P. Liu, L. Sun, F. Xu, *ACS Nano* **2024**, *18*, 19369.
[141] L. Shangguan, Y. Ran, Z. Lu, Y. Gao, L. Shi, L. He, L. Sun, *Nano Res.* **2023**, *16*, 5695.
[142] Y. Wang, M. Zhang, Z. Xue, X. Chen, Y. Mei, P. K. Chu, Z. Tian, X. Wu, Z. Di, *Small* **2022**, *18*, 2200913.
[143] C.-H. Lee, H. Ryu, G. Nolan, Y. Zhang, Y. Lee, S. Oh, H. Cheong, K. Watanabe, T. Taniguchi, K. Kim, G.-H. Lee, P. Y. Huang, *Nano Lett.* **2023**, *23*, 677.
[144] L. Liao, K. Liu, H. Luo, Y. Yu, A. Guo, W. Lin, F. Xia, Q. Zhang, X. Su, X. Tang, N. Wang, J. Wu, *ACS Nano* **2024**, *18*, 31995.
[145] K. Yu, W. Zhao, X. Wu, J. Zhuang, X. Hu, Q. Zhang, J. Sun, T. Xu, Y. Chai, F. Ding, L. Sun, *Nano Res.* **2018**, *11*, 2809.
[146] S. Wang, H. Sawada, Q. Chen, G. G. D. Han, C. Allen, A. I. Kirkland, J. H. Warner, *ACS Nano* **2017**, *11*, 9057.
[147] M. F. Crook, C. Laube, I. A. Moreno-Hernandez, A. Kahnt, S. Zahn, J. C. Ondry, A. Liu, A. P. Alivisatos, *J. Am. Chem. Soc.* **2021**, *143*, 11703.
[148] W. Wang, T. Xu, J. Chen, J. Shangguan, H. Dong, H. Ma, Q. Zhang, J. Yang, T. Bai, Z. Guo, H. Fang, H. Zheng, L. Sun, *Nat. Mater.* **2022**, *21*, 859.
[149] S. Lee, N. M. Schneider, S. F. Tan, F. M. Ross, *ACS Nano* **2023**, *17*, 5609.
[150] J. Korpanty, L. R. Parent, N. C. Gianneschi, *Nano Lett.* **2021**, *21*, 1141.
[151] Qi Zheng, J. Shangguan, X. Li, Q. Zhang, K C. Bustillo, L.-W. Wang, J. Jiang, H. Zheng, *Nano Lett.* **2021**, *21*, 6640.
[152] W. Wei, H. Zhang, W. Wang, M. Dong, M. Nie, L. Sun, F. Xu, *ACS Appl. Mater. Interfaces* **2019**, *11*, 24478.
[153] H. Ye, F. Yang, Y. Sun, R. Wang, *Small Methods* **2022**, *6*, 2200171.
[154] J. Hong, J.-H. Bae, H. Jo, H.-Y. Park, S. Lee, S. J. Hong, H. Chun, M. K. Cho, J. Kim, J. Kim, Y. Son, H. Jin, J.-Y. Suh, S.-C. Kim, H.-K. Roh, K. H. Lee, H.-S. Kim, K. Y. Chung, C. W. Yoon, K. Lee, S. H. Kim, J.-P. Ahn, H. Baik, G. H. Kim, B. Han, S. Jin, T. Hyeon, J. Park, C. Y. Son, Y. Yang, et al., *Nature* **2022**, *603*, 631.
[155] M. Ye, T. Xu, M. Liu, Y. Zhu, D. Yuan, H. Zhang, M. Qin, L. Sun, *Nano Lett.* **2023**, *23*, 7319.
[156] Y. Zhou, A. S. Powers, X. Zhang, T. Xu, K. Bustillo, L. Sun, H. Zheng, *Nanoscale* **2017**, *9*, 13915.
[157] L. Liu, K. Kluherz, B. Jin, D. R. Gamelin, J. J. De Yoreo, M. L. Sushko, *Nano Lett.* **2024**, *24*, 3299.
[158] Y. Zhong, T. C. Moore, T. Dwyer, A. Butrum-Griffith, V. R. Allen, J. Chen, Y. Wang, F. Cheng, S. C. Glotzer, X. Ye, *Nat. Chem. Eng.* **2024**, *1*, 532.
[159] C. Yan, D. Byrne, J. C. Ondry, A. Kahnt, I. A. Moreno-Hernandez, G. A. Kamat, Z.-J. Liu, C. Laube, M. F. Crook, Y. Zhang, P. Ercius, A. P Alivisatos, *Sci. Adv.* **2022**, *8*, abq1700.
[160] H. Hu, R. Yang, Z. Zeng, *ACS Nano* **2024**, *18*, 12598.
[161] Y. Li, H. Xu, Q. Ning, S. Li, J. Wang, J. Wang, Z. Hu, J. Tian, X. Li, Y. Han, Y. Zhu, *Adv. Funct. Mater.* **2024**, *34*, 2401361.
[162] S.-Y. Lee, J. Shangguan, J. Alvarado, S. Betzler, S J. Harris, M M. Doeff, H. Zheng, *Energy Environ. Sci.* **2020**, *13*, 1832.

[163] Q. Zhang, Z. Song, X. Sun, Y. Liu, J. Wan, S. B. Betzler, Q. Zheng, J. Shangguan, K. C. Bustillo, P. Ercius, P. Narang, Y. Huang, H. Zheng, *Nature* **2024**, *630*, 643.
[164] C. B. Maliakkal, E K. Mårtensson, M. U. Tornberg, D. Jacobsson, A. R. Persson, J. Johansson, L. R. Wallenberg, K. A. Dick, *ACS Nano* **2020**, *14*, 3868.
[165] Y.-C. Chou, C.-Y. Wen, M. C. Reuter, D. Su, E. A. Stach, F. M. Ross, *ACS Nano* **2012**, *6*, 6407.
[166] Y. Wang, L. Qiu, L. Zhang, D.-M. Tang, R. Ma, Y. Wang, B. Zhang, F. Ding, C. Liu, H.-M. Cheng, *ACS Nano* **2020**, *14*, 16823.
[167] X. Zhao, S. Sun, F. Yang, Y. Li, *Acc. Chem. Res.* **2022**, *55*, 3334.
[168] F. Yang, H. Zhao, X. Wang, X. Liu, Q. Liu, X. Liu, C. Jin, R. Wang, Y. Li, *J. Am. Chem. Soc.* **2019**, *141*, 5871.
[169] Y. Liu, L. Xu, L. Zhang, Z. Dong, S. Wang, L. Luo, *ACS Appl. Mater. Inter.* **2020**, *12*, 52201.
[170] P. L. Hansen, J. B. Wagner, S. Helveg, J. R. Rostrup-Nielsen, B. S. Clausen, H. Topsøe, *Science* **2002**, *295*, 2053.
[171] B. Zhu, J. Meng, W. Yuan, X. Zhang, H. Yang, Y. Wang, Y. Gao, *Angew. Chem., Int. Ed.* **2020**, *59*, 2171.
[172] K. Koo, Y. Liu, Y. Cheng, Z. Cai, X. Hu, V. P. Dravid, *Chem. Mater.* **2024**, *36*, 4078.
[173] Y. Jiang, H. Li, Z. Wu, W. Ye, H. Zhang, Y. Wang, C. Sun, Z. Zhang, *Angew. Chem., Int. Ed.* **2016**, *55*, 12427.
[174] X. Zhang, J. Meng, B. Zhu, W. Yuan, H. Yang, Z. Zhang, Y. Gao, Y. Wang, *Chem. Commun.* **2018**, *54*, 8587.
[175] S. Dai, Y. You, S. Zhang, W. Cai, M. Xu, L. Xie, R. Wu, G. W. Graham, X. Pan, *Nat. Commun.* **2017**, *8*, 204.
[176] S. Han, G.-J. Xia, C. Cai, Q. Wang, Y.-G. Wang, M. Gu, J. Li, *Nat. Commun.* **2020**, *11*, 552.
[177] S. Han, C. Cai, G.-J. Xia, C. Sun, X. Shi, W. Zhou, J. Li, Y.-G. Wang, M. Gu, *Inorg. Chem.* **2020**, *59*, 14415.
[178] A. Baldi, T. C. Narayan, A. L. Koh, J. A. Dionne, *Nat. Mater.* **2014**, *13*, 1143.
[179] T. C. Narayan, F. Hayee, A. Baldi, A. Leen Koh, R. Sinclair, J. A. Dionne, *Nat. Commun.* **2017**, *8*, 14020.
[180] X. Zhang, S. Han, B. Zhu, G. Zhang, X. Li, Y. Gao, Z. Wu, B. Yang, Y. Liu, W. Baaziz, O. Ersen, M. Gu, J. T. Miller, W. Liu, *Nat. Catal.* **2020**, *3*, 411.
[181] J. Gao, X. Luo, F. Fang, J. Sun, *Int. J. Extrem. Manuf.* **2022**, *4*, 012001.
[182] P. M. Pelz, S. M. Griffin, S. Stonemeyer, D. Popple, H. DeVyldere, P. Ercius, A. Zettl, M. C. Scott, C. Ophus, *Nat. Commun.* **2023**, *14*, 7906.
[183] Z. Chen, Y. Jiang, Y.-T. Shao, M. E. Holtz, M. Odstrcil, M. Guizar-Sicairos, I. Hanke, S. Ganschow, D. G. Schlom, D. A. Muller, *Science* **2021**, *372*, 826.
[184] B. Yuan, Z. Wang, S. Zhang, C. Hofer, C. Gao, T. Chennit, H. Shi, X. Wu, Y. Han, L. Dou, Y. Yu, T. J. Pennycook, *Nature* **2025**, *647*, 364.

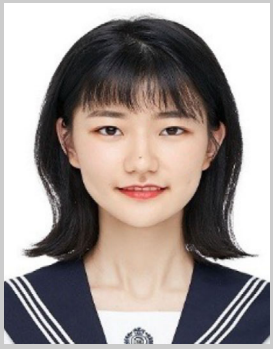

Mingrui Zhou is currently a Ph.D. student at the SEU-FEI Nano-Pico Center, Key Laboratory of MEMS of the Ministry of Education of the Southeast University. Her research focuses on characterization and fabrication of nanoscale materials based on in situ transmission electron microscopy.

Chen Li is currently a Ph.D. student at Southeast University. His main research interests are in situ transmission electron microscopy characterization, 2D materials, and memristors.

Hua Hong received his B.S. from Polytechnic University of Turin, Italy, and Ph.D. from Rutgers University, USA. Currently, he is an associate professor at Southeast University, China. His primary research interest lies in the synthesis and processing of advanced materials, with a focus related to nanostructured carbon. He is dedicated to the development and optimization of innovative nanomaterial systems to enable the mass production of materials with tailored properties, aiming for applications centered on electronics and bioelectronic devices.

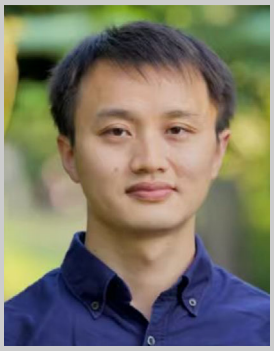

Hubiao Huang received his M.S. degree in 2014 from Zhejiang University, China, under the supervision of Prof. Xinsheng Peng. He then moved to Japan and obtained his Ph.D. degree in 2017 from the University of Tokyo under the supervision of Prof. Takuzo Aida. After working as a JSPS Research Fellow at the University of Tokyo until 2019, he joined RIKEN as a researcher and later held concurrent roles as an assistant professor at the University of Tokyo and core scientist in the TRIP project. In 2024, he became a professor at Southeast University, China. His research interests center on supramolecular materials, including mechanically strong plastics, chiral crystals, and nanoporous architectures for applications in energy, separation, and biomedicine.

Qiubo Zhang received his Ph.D. in microelectronics and solid electronics from Southeast University, China. After that, he worked as a postdoc at Lawrence Berkeley National laboratory from 2019 to 2025, and worked as a research scientist in University of California, Berkeley. Currently, he is a professor at the Southeast University. His research interests are centered on understanding how dynamics of solid-liquid interfaces impact the physical and chemical processes of advanced materials.

Kuibo Yin received the Ph.D. degree in materials science from Nanjing University, Nanjing, China, in 2008. He is currently a professor at Southeast University, Nanjing. His research interests focus on the characterization and application of energy storage materials and novel 2-D materials.

Li Zhong received his Bachelor's and Master's degrees in Materials Science and Engineering from Beihang University, and his Ph.D. in Mechanical Engineering and Materials Science from University of Pittsburgh. He is currently a professor at School of Integrated Circuits, Southeast University. His research interests include atomistic perspectives on materials properties, structural design, in-situ characterization, underlying mechanisms, and performance modulation for atomic-scale manufacturing.

Chao Zhu received his Bachelor's degree in Physics from Nanjing University and his Ph.D. in Physics from the Hong Kong University of Science and Technology. He conducted postdoctoral research at institutions including the School of Electronic Science and Engineering at Southeast University and the School of Materials Science and Engineering at Nanyang Technological University in Singapore. Currently, he is a full-time professor at Southeast University, Director of Atomic-Scale Manufacturing Research Center for Nano Devices. His long-term research focuses on the atomic scale investigation of two-dimensional materials and devices.

Tao Xu received his B.S. (2009) and Ph.D. (2016) from Southeast University under the supervision of Prof. Litao Sun. After completing his doctoral studies in the School of Electronic Science and Engineering, he joined the faculty and was promoted to professor in 2025. His current research interests focus on the atomic-scale structural evolution of electronic materials under various stimuli, as well as the development of fabrication methodologies for nanoscale materials.

Litao Sun received his Ph.D. degree in 2005 from the Shanghai Institute of Applied Physics, Chinese Academy of Sciences, and carried out postdoctoral research at the University of Mainz, Germany, from 2005 to 2008. He subsequently joined Southeast University as a professor, where he currently serves as Director of the Key Laboratory of Micro-Electro-Mechanical Systems of Ministry of Education and as Vice President of Southeast University. His research focuses on nano-electronic materials and devices, visualized atomic-scale manufacturing, and in-situ electron microscopy.